

## Long-timescale motions in glycerol-monopalmitate lipid bilayers investigated using molecular dynamics simulation



Monika Laner<sup>a</sup>, Bruno A.C. Horta<sup>a,b,c</sup>, Philippe H. Hünenberger<sup>a,\*</sup>

<sup>a</sup> Laboratory of Physical Chemistry, ETH Zürich, Zürich, Switzerland

<sup>b</sup> Dpto. de Engenharia Elétrica, PUC-Rio, Rio de Janeiro, Brazil

<sup>c</sup> Dpto. de Ciências Biológicas, UEGO, Rio de Janeiro, Brazil

### ARTICLE INFO

#### Article history:

Accepted 30 October 2014

Available online 8 November 2014

#### Keywords:

Molecular dynamics

Lipid bilayer

Monoglyceride

Phase transitions

Tilt precession

Flip-flop

### ABSTRACT

The occurrence of long-timescale motions in glycerol-1-monopalmitate (GMP) lipid bilayers is investigated based on previously reported 600 ns molecular dynamics simulations of a  $2 \times 8 \times 8$  GMP bilayer patch in the temperature range 302–338 K, performed at three different hydration levels, or in the presence of the cosolutes methanol or trehalose at three different concentrations. The types of long-timescale motions considered are: (i) the possible phase transitions; (ii) the precession of the relative collective tilt-angle of the two leaflets in the gel phase; (iii) the *trans*–*gauche* isomerization of the dihedral angles within the lipid aliphatic tails; and (iv) the flipping of single lipids across the two leaflets. The results provide a picture of GMP bilayers involving a rich spectrum of events occurring on a wide range of timescales, from the 100-ps range isomerization of single dihedral angles, via the 100-ns range of tilt precession motions, to the multi- $\mu$ s range of phase transitions and lipid-flipping events.

© 2014 Elsevier Inc. All rights reserved.

## 1. Introduction

The cell membrane defines the boundary of a cell and works as the separating barrier and first interaction site of the cell with its surroundings [1]. The basic component of this membrane is a lipid bilayer [2–5]. Several phases are known for lipid bilayers in aqueous environments [6,7], their prevalence being determined by the types of the lipid molecules, their concentrations, the possible presence of cosolutes (CSLs), as well as pressure and temperature. The corresponding phase-transition temperatures and mechanisms are of fundamental importance for both biology and technology [6,8].

The biologically most relevant phases of lipid bilayers are the liquid crystal (LC) and the gel (GL) phases [9,10]. In the presence of short-chain aliphatic alcohols, a third type of phase can appear, the interdigitated (ID) phase [11–13]. These three phases are sometimes referred to as  $L_\alpha$ ,  $L_\beta$  (or  $L_{\beta'}$ ), and  $L_{\beta I}$ , for LC, GL and ID, respectively [9], and can be distinguished by the arrangement of the lipids within the bilayer and by differences in the area per lipid, in the bilayer thickness, in the distribution of the headgroup

and tail atoms along the bilayer normal, and in the methylene carbon–hydrogen order parameters [6,14,15].

In the LC phase, the tails are conformationally disordered, involving a mixture of *trans* and *gauche* conformations. The methylene groups present low order parameters [9] and no preferential collective orientation of the chains relative to the bilayer normal (collective tilting) is observed.

In the GL phase, the aliphatic lipid tails are arranged in nearly all-*trans* conformations and the methylene groups present high order parameters [9]. In the  $L_{\beta'}$  form of the GL phase, the tails are tilted with respect to the bilayer normal [9,10]. In the  $L_\beta$  form, the tails are oriented perpendicularly to the bilayer midplane [16]. The prevalence of either  $L_{\beta'}$  or  $L_\beta$  is determined by the ratio of the effective headgroup to tail cross-sections [16], a high ratio favoring tilting [9,16–18], i.e.  $L_{\beta'}$  over  $L_\beta$ . Compared to the LC phase, the GL phase is also laterally more compact and transversely more expanded, the difference being most pronounced when the GL phase involves a low tilt angle [18,19].

In the ID phase, the aliphatic tails of the two leaflets interpenetrate in such a way that the terminal methyl groups of one leaflet are located close to the headgroups of the other [19–25]. The ID bilayer presents a lateral expansion and transversal compaction comparable to the LC phase, along with a tight chain packing and nearly all-*trans* conformations of the tails similar to the GL phase. To our knowledge, the extent of tilting of a bilayer in the ID phase has not been determined experimentally. However, considering that the

\* Corresponding author at: Laboratory of Physical Chemistry, ETH Hönggerberg, HCI, CH-8093 Zürich, Switzerland. Tel.: +41 44 632 55 03; fax: +41 44 632 10 39.

E-mail addresses: [monika.laner@igc.phys.chem.ethz.ch](mailto:monika.laner@igc.phys.chem.ethz.ch) (M. Laner), [bruno.horta@gmail.com](mailto:bruno.horta@gmail.com) (B.A.C. Horta), [phil@igc.phys.chem.ethz.ch](mailto:phil@igc.phys.chem.ethz.ch) (P.H. Hünenberger).

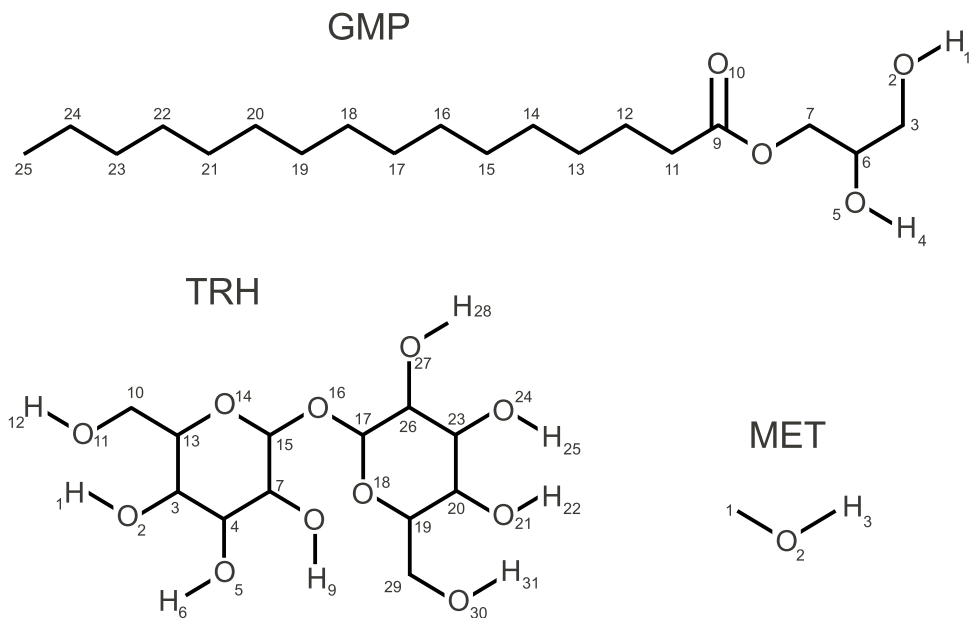


**Fig. 1.** Chemical structures of the monoglyceride and cosolutes considered in the present study. The compounds are the lipid glycerol-1-monopalmitate (GMP) and the cosolutes (CSLs) trehalose (TRH) and methanol (MET). The numbering refers to the GROMOS molecular topology used in the simulations. See Ref. [19] and Suppl. Mat. therein for detailed force-field information.

headgroup spacing is largely increased compared to that in the GL phase, it seems reasonable to assume that the ID phase generally presents little or no tilting, a suggestion supported by simulations of monoglyceride bilayers [19]. The methylene order parameters are typically even higher in the ID than in the GL phase [26–28], which results from both a reduced tilting and a tighter chain packing [19,29].

Atomistic molecular dynamics (MD) simulations have greatly contributed to the characterization and understanding of the structure, thermodynamics and dynamics of lipid bilayers under various conditions [19,30–49]. These simulations provide information at a spatial (atomic level) and temporal (femtosecond) resolution inaccessible to experiment, concerning system sizes ( $\sim 10$  nm) and timescales ( $\sim 1\ \mu\text{s}$ ) already relevant for the evaluation of thermodynamic properties *via* statistical mechanics and the comparison with experimental data. Most of these studies have been carried out in the context of biologically relevant lipids, typically diglycerides with functionalized headgroups such as dipalmitoylphosphatidylcholine (DPPC) [31,33–35,37,38,41,42,45,47]. However, these lipids remain relatively challenging to simulate, owing to difficulties in the force-field design [50,51] and treatment of electrostatic interactions [50,52–57], and to the slow convergence of system properties with respect to both system size [18,49–51,58–60] and simulation timescale [18,58,61–63].

For this reasons, it is also of interest to consider less complex bilayer systems such as monoglyceride lipid systems [19,43,47–49,64,65]. In addition to being relevant in the context of prebiotic research [66,67] and technological applications [68,69], these lipids present a number of key advantages compared to e.g. DPPC for a computational investigation of lipid phase transitions: (i) the presence of only one aliphatic tail per headgroup, leading to a faster relaxation; (ii) the limited role of electrostatic interactions (uncharged, non-zwitterionic and moderately polar headgroup); (iii) the absence of a ripple phase [70] as an intermediate state between the GL and LC phases; and (iv) the availability of experimental structural and thermodynamic data [14,68,69,71–77].

In a series of previous studies by our group, glycerol-1-monopalmitate (GMP; Fig. 1) was chosen as a test system to investigate the phase characteristics and phase-transition

properties of a simple model lipid [19,43,47–49,64,65]. In particular, the effects of the hydration level and of the possible presence of the CSLs methanol and trehalose (MET and TRH, respectively; Fig. 1) on the bilayer properties and on the main transition temperature  $T_m$  for the GL  $\leftrightarrow$  LC transition were investigated in detail [19]. The three phases LC, GL (tilted) and ID (only in the presence of MET) of GMP bilayers, as well as their interconversion, were observed in these simulations, as illustrated in Fig. 2. This previous study was based on 83 MD simulations, each of 600 ns duration, of a GMP bilayer patch of  $2 \times 8 \times 8$  lipids carried out at different temperatures in the range of 302–338 K, either in the absence of CSL at three different hydration levels (simulations previously reported in Ref. [49]) or in the presence of MET or TRH at three different concentrations.

In the present article, these simulations are further analyzed to investigate the occurrence of long-timescale motions in the bilayer and the influence of hydration and CSLs on these motions. The slow motions considered are: (i) the possible phase transitions; (ii) the precession of the relative collective tilt-angle of the two leaflets in the GL phase; (iii) the *trans-gauche* isomerization of the dihedral angles within the lipid tails; and (iv) the flipping of single lipids across the two leaflets.

## 2. Methods

### 2.1. Molecular dynamics simulations

All the MD simulations considered were reported previously in Ref. [19]. The corresponding force-field information and simulation details can be found therein, and only the essential points will be repeated here.

The MD simulations were performed using the GROMOS MD++ program [78–80], with the 53A6<sub>OXY</sub> force field [81] for GMP, TRH and MET, along with the simple point charges (SPC) water model [82]. They were carried out under periodic boundary conditions based on rectangular boxes containing a hydrated GMP bilayer patch of  $2 \times 8 \times 8$  lipid molecules in the  $xy$ -plane, leading to a total number of 128 lipid molecules in the systems. Both leaflets consisted of a racemic mixture of the *R* and *S* enantiomers of the GMP molecule. A variable number of CSL molecules was added:

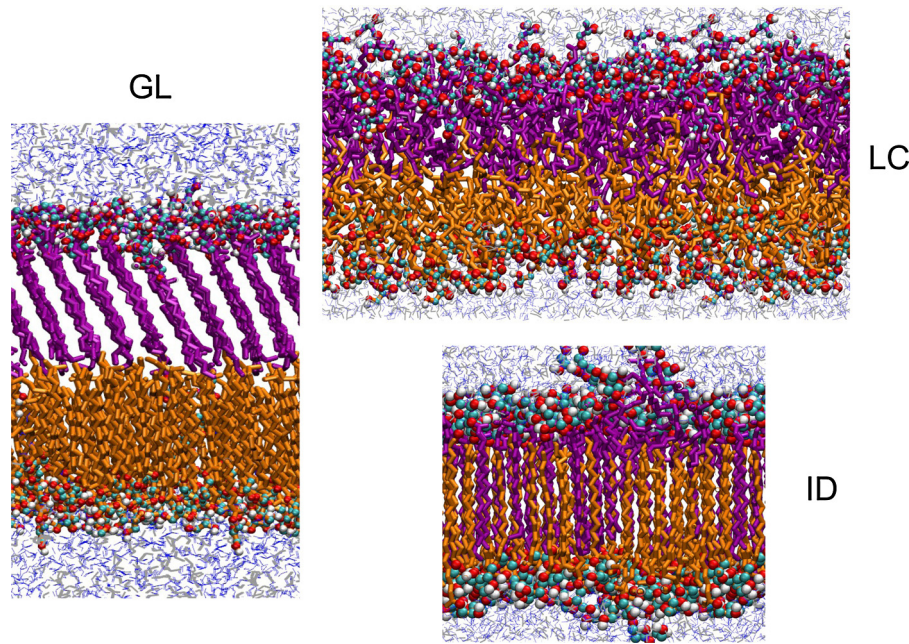


**Fig. 2.** Illustrative configurations for the different phases of a GMP lipid bilayer. Shown are trajectory snapshots corresponding to the three phases GL (at 60 ns), LC (at 240 ns) and ID (at 600 ns) occurring in simulation M<sub>E</sub>F<sub>GL</sub>310. The lipids are colored in orange and purple to distinguish the two leaflets (bottom and top, respectively), MET is displayed in gray and water molecules in blue. The atoms of the headgroup are colored according to the element (C1, C2, C3: light blue, O1, O2, O3: red, and H1, H2: white). Note that the structure for LC is shown along the x-axis of the box, while the structures for GL and ID were rotated around the z-axis to highlight the structural characteristics (alignment or interdigitation). The simulation labels and conditions are summarized in Table 1. (For interpretation of the references to color in this figure legend, the reader is referred to the web version of the article.)

(i) none (simulations labeled P<sub>N</sub>, i.e. pure aqueous lipid); (ii) 53 molecules of TRH (simulations labeled T<sub>N</sub>); and (iii) either 120, 240 or 480 molecules of MET (simulations labeled M<sub>L</sub>, M<sub>M</sub> and M<sub>E</sub>, respectively, i.e. low, medium or elevated MET content).

For both the pure-lipid simulations (P<sub>N</sub>) and the simulations in the presence of TRH (T<sub>N</sub>), three hydration levels were considered, distinguished by the letters F (full), H (half), or Q (quarter), respectively. The full hydration regime was defined by a 36% w/w water content (6.7 water molecules per lipid). Accordingly, the numbers of water molecules in the simulated systems were set to 853 (F), 427 (H) and 213 (Q). The simulations in the presence of MET (M<sub>L</sub>, M<sub>M</sub> and M<sub>E</sub>) were all carried out at full hydration.

A total number of 83 simulations were carried out, differing by: (i) the possible presence and type of the CSL (P vs. T vs. M); (ii) the number of CSL molecules in the system (N vs. L vs. M vs. E); (iii) the hydration level (F vs. H vs. Q); (iv) the initial configuration (GL vs. LC); and (v) the temperature T (from 302, 306 or 318 K, depending on the system, to 338 K in steps of 4 K). Only a subset of the possible combinations was considered, the corresponding systems and conditions being summarized in Table 1. Each of the 83 simulations is uniquely identified by a string consisting in sequence of the letters P, T or M (system), N, L, M or E (CSL content; subscript), F, H or Q (hydration level), and GL or LC (initial configuration; subscript), followed by the temperature T. The generation of the initial configurations and the equilibration procedure are described in Ref. [19].

All simulations were carried out at constant temperature (T) and pressure (1 bar) using the weak-coupling method [83] for a duration of 600 ns after equilibration. They relied on a twin-range cutoff scheme [84,85] and reaction-field electrostatics [86,87], with short- and long-range cutoff distances set to 0.9 and 1.4 nm, respectively, an update frequency of 5 timesteps for the short-range pairlist and intermediate-range interactions, and a solvent reaction-field permittivity of 61. Configurations were saved to file every 10 ps for analysis.

## 2.2. Trajectory analysis

The basic analyses of the simulated trajectories and the corresponding results were described already in Ref. [19]. To characterize the occurrence of long-timescale processes, the data was further analyzed in terms of the following properties: (i) phase-assignment descriptor; (ii) single-lipid and collective tilt angles; (iii) populations of *trans* conformers for the tail dihedral angles; and (iv) occurrences of lipid-flipping events.

The phase-assignment descriptor ascribes a phase to each trajectory configuration, so as to monitor the occurrence of transitions and the extent of sampling of the different phases. This is done by taking into account the area per lipid, the headgroup-headgroup distance across the bilayer, and the relative positions of the methyl groups of the bottom and top leaflets as described in Ref. [19] (see Eq. (1) therein). The resulting descriptor assigns single trajectory configurations to either the LC, GL or ID phase, or to an unknown (UN) type if the structural observables fail to fall in appropriate ranges.

The analysis of the lipid tilt angles was carried out based on single-lipid head-tail vectors  $\mathbf{v}_n$  ( $n = 1, \dots, 128$ ), defined by the ester carbonyl carbon atom and the terminal methyl group of each lipid, and relied on a bilayer-linked system of polar angles as illustrated in Fig. 3a. In a given trajectory configuration, the single-lipid apical tilt angle  $\theta_n$  is defined as the angle between  $\mathbf{v}_n$  and the z-axis of the box (along the bilayer normal, pointing from bottom to top leaflet). This angle spans the range 0–180°, and is typically smaller than 90° for the bottom leaflet and larger than 90° for the top leaflet. The single-lipid azimuthal tilt angle  $\phi_n$  is defined as the angle between the projection of  $\mathbf{v}_n$  in the xy-plane (bilayer plane) and the x-axis of the box. This angle spans the range of 0–360°. The apical angle  $\theta_n$  can be averaged over the lipids of the bottom and top leaflets separately, resulting in values  $\theta_{bot}$  and  $\theta_{top}$ , respectively. Alternatively, the average of the angles  $\theta_n$  (bottom leaflet) or 180°– $\theta_n$  (top leaflet) over all lipids of the bilayer is noted  $\theta$ , and the corresponding

**Table 1**

Simulated systems and simulation conditions. For each simulation, the different columns report the simulation label, the type of cosolute (CSL) molecule (none, TRH for trehalose, or MET for methanol), the number  $n_C$  of CSL molecules, the CSL concentration  $c_C$  (by weight relative to the lipids), the hydration level relative to full hydration (F, H or Q for full, half, or quarter), the number  $n_W$  of water molecules, the water concentration  $c_W$  (by weight relative to the lipids), the starting configuration (GL for gel or LC for liquid crystal) and the reference temperature  $T$ . In all cases, the simulations involve a glycerol-1-monopalmitate (GMP) bilayer patch of  $2 \times 8 \times 8$  lipids and are carried out for 600 ns at the reference pressure  $P = 1$  bar. For compactness, a single entry is provided for each set of simulations carried out at different temperatures  $T$  (value in Kelvin noted generically  $T$  in the simulation label). For example the notation  $T \in \{318\text{--}338\}$  indicates a set of six simulations at temperatures  $T$  ranging from 318 to 338 K in steps of 4 K, and the notation  $T \in \{318, 338\}$  indicates a set of two simulations carried out at temperatures  $T$  of 318 and 338 K.

Simulation	CSL	$n_C$	$c_C$ [% w/w]	Hydration	$n_W$	$c_W$ [% w/w]	Starting configuration	$T$ [K]
$P_N F_{GL} T$	None	0	—	F	853	36.3	GL	$T \in \{318\text{--}338\}$
$P_N F_{LC} T$	None	0	—	F	853	36.3	LC	$T \in \{318, 338\}$
$P_N H_{GL} T$	None	0	—	H	427	18.2	GL	$T \in \{318\text{--}338\}$
$P_N H_{LC} T$	None	0	—	H	427	18.2	LC	$T \in \{318, 338\}$
$P_N Q_{GL} T$	None	0	—	Q	213	9.1	GL	$T \in \{318\text{--}338\}$
$P_N Q_{LC} T$	None	0	—	Q	213	9.1	LC	$T \in \{318, 338\}$
$T_N F_{GL} T$	TRH	53	42.9	F	853	36.3	GL	$T \in \{318\text{--}338\}$
$T_N F_{LC} T$	TRH	53	42.9	F	853	36.3	LC	$T \in \{318, 338\}$
$T_N H_{GL} T$	TRH	53	42.9	H	427	18.2	GL	$T \in \{318\text{--}338\}$
$T_N H_{LC} T$	TRH	53	42.9	H	427	18.2	LC	$T \in \{318, 338\}$
$T_N Q_{GL} T$	TRH	53	42.9	Q	213	9.1	GL	$T \in \{318\text{--}338\}$
$T_N Q_{LC} T$	TRH	53	42.9	Q	213	9.1	LC	$T \in \{318, 338\}$
$M_L F_{GL} T$	MET	120	9.1	F	853	36.3	GL	$T \in \{302\text{--}338\}$
$M_L F_{LC} T$	MET	120	9.1	F	853	36.3	LC	$T \in \{302, 338\}$
$M_M F_{GL} T$	MET	240	18.2	F	853	36.3	GL	$T \in \{302\text{--}338\}$
$M_M F_{LC} T$	MET	240	18.2	F	853	36.3	LC	$T \in \{302, 338\}$
$M_E F_{GL} T$	MET	480	36.4	F	853	36.3	GL	$T \in \{306\text{--}338\}$
$M_E F_{LC} T$	MET	480	36.4	F	853	36.3	LC	$T \in \{306, 338\}$

standard deviation across lipids  $\gamma_\theta$ . A common averaging is justified by the similar properties of the two leaflets in terms of  $\theta$  (see Section 3.2). The value of  $\theta$  characterizes the average tilt of the single-lipid head-tail vectors relative to a leaflet-to-midplane axis, and is typically smaller than 90°. A corresponding averaging of the single-lipid azimuthal angles  $\phi_n$  makes little sense, considering that these angles typically span a large fraction of the periodic range 0–360°.

In addition, collective tilt angles are defined separately for the bottom and top leaflets of the bilayer by considering the corresponding vector sums of single-lipid head-tail vectors,  $\mathbf{V}_{bot}$  and  $\mathbf{V}_{top}$ , see Fig. 3b. The collective apical tilt angles  $\Theta_{bot}$  and  $\Theta_{top}$

are defined as the angles between  $\mathbf{V}_{bot}$  and  $\mathbf{V}_{top}$ , respectively, and the z-axis. The collective azimuthal tilt angles  $\Phi_{bot}$  and  $\Phi_{top}$  are defined as the angles between the projections of  $\mathbf{V}_{bot}$  and  $\mathbf{V}_{top}$ , respectively, in the xy-plane and the x-axis. The average of  $\Theta_{bot}$  and  $180^\circ - \Theta_{top}$  is noted  $\Theta$ . A common averaging is again justified by the similar properties of the two leaflets in terms of  $\Theta$  (see Section 3.2). In terms of  $\Phi$ , however, the two leaflets typically differ, and averaging  $\Phi_{bot}$  and  $\Phi_{top}$  makes little sense.

The analysis of the lipid-tail dihedral-angle conformations was performed considering the 13 successive dihedral angles  $\omega_k$  of the acyl chains, labeled  $\omega_1$  ( $C_9-C_{11}-C_{12}-C_{13}$ , where  $C_9$  is the ester carbonyl carbon atom) to  $\omega_{13}$  ( $C_{22}-C_{23}-C_{24}-C_{25}$ , where  $C_{25}$  is the

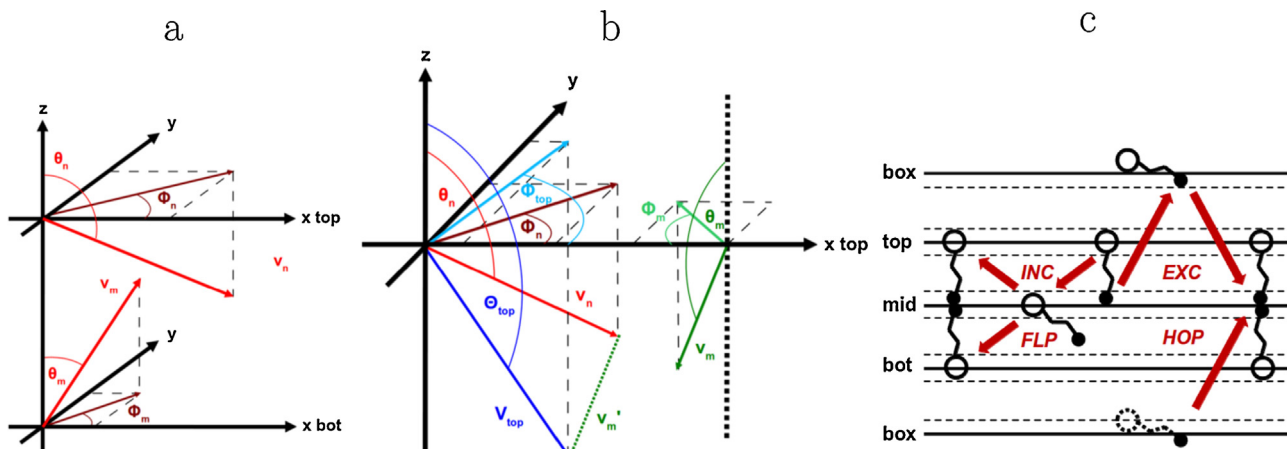


**Fig. 3.** Definitions of the tilt angles and lipid-flipping events considered in the analysis of the simulations. (a) Illustration of the single-lipid apical and azimuthal tilt angles for a lipid  $m$  of the bottom leaflet (angles  $\theta_m$  and  $\phi_m$ ) and a lipid  $n$  of the top leaflet (angles  $\theta_n$  and  $\phi_n$ ). The apical angle is defined as the angle between the head-tail vectors  $\mathbf{v}_m$  or  $\mathbf{v}_n$  and the z-axis (bilayer normal, pointing from bottom to top leaflet). The azimuthal angle is defined as the angle between the projection of  $\mathbf{v}_m$  or  $\mathbf{v}_n$  in the xy-plane (bilayer plane) and the x-axis (one edge of the simulation box). The averages of  $\theta_m$  or  $\theta_n$  over the bottom and top leaflets are noted  $\theta_{bot}$  and  $\theta_{top}$ , respectively. The average of  $\theta_m$  and  $180^\circ - \theta_n$  over all lipids is noted  $\theta$  (standard deviation over lipids  $\gamma_\theta$ ). (b) Illustration of the collective apical and azimuthal tilt angles  $\Theta_{top}$  and  $\Phi_{top}$  of the top leaflet, considering only two lipids  $m$  and  $n$  of this leaflet for simplicity. The apical angle is defined as the angle between the vector sum  $\mathbf{V}_{top}$  of the head-tail vectors and the z-axis. The azimuthal angle is defined as the angle between the projection of  $\mathbf{V}_{top}$  in the xy-plane and the x-axis. The average of  $\Theta_{bot}$  and  $180^\circ - \Theta_{top}$  is noted  $\Theta$ . (c) Illustration of the lipid-flipping events considered, as defined by the lipid head and tail positions relative to successive layers along the z-axis via Eqs. (1) and (2). The layers are defined by ranges of half-width  $\Delta z$  around the planes of the box wall (box), bottom headgroups (bot), bilayer midplane (mid), and top headgroups (top). The special events include: incursions (INC; lipid headgroup enters the midplane and exits to the same leaflet); flips (FLP; lipid headgroup changes leaflet via the bilayer midplane); excursions (EXC; lipid tail enters the box-wall plane and exits to the same leaflet); hops (HOP; lipid tail changes leaflet via the box-wall plane).

terminal methyl group), see Fig. 1. The corresponding *trans* populations  $\alpha_k^{bot}$  and  $\alpha_k^{top}$  were determined separately for the bottom and top leaflets, by considering a window of  $\pm 60^\circ$  around the *trans* value of  $180^\circ$ . These *trans* populations were also compared to the carbon–hydrogen order parameters  $S_{CH}(C_n)$  of the tail methylene groups  $n=11–24$  (see Fig. 1), which were analyzed as described in Ref. [49].

The analysis of lipid-flipping events rests on the observation that specific lipids undergo moves from one leaflet either back to the same leaflet or to the opposite leaflet of the bilayer, and either *via* the interior of the membrane (bilayer midplane) or *via* the exterior of the membrane (aqueous phase, *i.e.* in the simulations, wall of the computational box perpendicular to the  $z$ -axis). Considering the events involving a change of leaflet, the interior path is commonly referred to as a flip-flop [88–91] or simply a flip [92], the exterior path being referred to here as a hop. Considering the events involving no change of leaflet, the brief exit of a lipid tail terminus into the aqueous phase (box wall) or visit of a lipid head-group to the bilayer midplane are referred to here as an excursion or an incursion, respectively. As illustrated in Fig. 3c, the monitoring of these events was performed by means of single-configuration lipid-location descriptors  $H_n$  for incursions and flips, and  $T_n$  for excursions and hops.

To identify incursions and flips, the descriptor  $H_n$  was defined for each lipid  $n$  as

$$H_n = \begin{cases} +1 & \text{if } z_{top} - \Delta z \leq z_n^h \leq z_{top} + \Delta z \\ 0 & \text{if } -\Delta z \leq z_n^h \leq +\Delta z \\ -1 & \text{if } z_{bot} - \Delta z \leq z_n^h \leq z_{bot} + \Delta z \end{cases}. \quad (1)$$

The parameters  $z_{bot}$  and  $z_{top}$  are calculated for a trajectory configuration by periodic gathering of the lipid atoms along the  $z$ -direction with the bilayer midplane (average of the  $z$ -coordinate of the 128 terminal methyl groups) at  $z=0$ , and measurement of the average  $z$ -coordinate of the 64 glycerol central carbon atoms (atom 6 in Fig. 1) of the bottom ( $z_{bot}$ ) and top ( $z_{top}$ ) leaflets, respectively. The variable  $z_n^h$  is the coordinate of the glycerol central carbon atom of lipid  $n$  along the  $z$ -axis. The half-width  $\Delta z$  of the three regions was set to 0.2 nm. Monitoring  $H_n$  as a function of time for all lipids provided unambiguous definitions for the two types of lipid-flipping events (see Fig. 3c). For a given lipid, each location-descriptor sequence  $-1 \rightarrow \{0\} \rightarrow +1$  or  $+1 \rightarrow \{0\} \rightarrow -1$  along the trajectory was counted as a flip and each sequence  $-1 \rightarrow \{0\} \rightarrow -1$  or  $+1 \rightarrow \{0\} \rightarrow +1$  was counted as an incursion, where  $\{0\}$  denotes any sequence with  $H_n=0$  or  $H_n$  undefined (*i.e.* excluding  $H_n=\pm 1$ ).

To identify excursions and hops, the descriptor  $T_n$  was defined for each lipid  $n$  as

$$T_n = \begin{cases} +2 & \text{if } z_n^t \leq -z_{box} + \Delta z \text{ or } z_n^t \geq z_{box} - \Delta z \\ +1 & \text{if } z_{top} - \Delta z \leq z_n^t \leq z_{top} + \Delta z \\ 0 & \text{if } -\Delta z \leq z_n^t \leq +\Delta z \\ -1 & \text{if } z_{bot} - \Delta z \leq z_n^t \leq z_{bot} + \Delta z \end{cases}. \quad (2)$$

The parameters  $z_{bot}$ ,  $z_{top}$  and  $\Delta z$  are defined as above, and the parameter  $z_{box}$  stands for the half-edge length of the simulation box along the  $z$ -axis in the configuration. The variable  $z_n^t$  is the coordinate of the terminal methyl group of lipid  $n$  along the  $z$ -axis (with  $-z_{box} < z_n^t \leq z_{box}$ ). Monitoring  $T_n$  as a function of time for all lipids provided unambiguous definitions for the two types of lipid-flipping events (see Fig. 3c). For a given lipid, each location-descriptor sequence  $0 \rightarrow \{-1\} \rightarrow \{+2\} \rightarrow \{+1\} \rightarrow 0$  or  $0 \rightarrow \{+1\} \rightarrow \{+2\} \rightarrow \{-1\} \rightarrow 0$  was counted as a hop and each sequence  $0 \rightarrow \{-1\} \rightarrow \{+2\} \rightarrow \{-1\} \rightarrow 0$  or  $0 \rightarrow \{+1\} \rightarrow \{+2\} \rightarrow \{+1\} \rightarrow 0$  was counted as an excursion.

**Table 2**

Possible occurrence of a phase transition during the different simulations. The simulations were started from a structure appropriate for the GL phase and carried out at reference temperatures ranging between  $T_{min}=302$  (systems  $M_L$  and  $M_M$ ), 306 (system  $M_E$ ) or 318 K (all other systems) and 338 K in steps of 4 K, or from a structure appropriate for the LC phase and carried out at reference temperatures  $T_{min}$  or 338 K. They differ by the different CSLs (P, T or M), numbers of CSL molecules (N, L, M, or E) and hydration levels (F, H or Q). A minus (–) indicates the absence of a transition, a cross (×) the presence of a GL → LC transition, a diamond (◊) the presence of a LC → ID transition and a square (□) the presence of a LC → UN transition. No LC → GL transition was observed in these simulations. All simulations present at most one transition, except  $M_E F_{GL} 310$ , which undergoes a transition to LC followed by a transition to ID. The simulation labels and conditions are summarized in Table 1.

Initial phase	$T$ [K]	$P_N$			$T_N$			M		
		F	H	Q	F	H	Q	L	M	E
GL	302							–	–	–
GL	306							–	–	–
GL	310							–	–	◊
GL	314							–	×	×
GL	318	–	–	–	–	–	–	×	×	×
GL	322	×	×	–	×	×	–	×	×	×
GL	326	×	×	×	×	×	×	×	×	×
GL	330	×	×	×	×	×	×	×	×	×
GL	334	×	×	×	×	×	×	×	×	×
GL	338	×	×	×	×	×	×	×	×	×
LC	$T_{min}$	–	–	–	–	–	–	□	◊	◊
LC	338	–	–	–	–	–	–	–	–	–

Again, the braces indicate any sequence alternating the indicated  $T_n$  value with  $T_n$  undefined (*i.e.* excluding any other  $T_n$  value).

### 3. Results and discussion

#### 3.1. Occurrence of phase transitions

Among the 83 simulations (Table 1), nearly all evidence none or a single GL → LC or LC → ID transition over 600 ns, as summarized in Table 2. The only two exceptions are simulations  $M_E F_{GL} 310$  (GL → LC followed by LC → ID) and  $M_L F_{LC} 302$  (transition to unassigned UN configurations, corresponding to the ID phase with some lipids extruded from the bilayer [19]). The occurrence of phase transitions, the phase-transition temperatures and the transition kinetics are discussed elsewhere [19,43,49,64,65], and will not be further considered. Phase transitions are merely mentioned here because they represent an important form of long-timescale event in these systems, with transition durations on the order of 2–10 ns, the transitions themselves being separated by much longer intervals [65], typically in the multi- $\mu$ s regime close to  $T_m$ .

Most of the discussion concerning other types of long-timescale motions, provided in Sections 3.2–3.4, focuses on the nine simulations initiated from a GL structure and carried out at the lowest temperatures considered (302 K for  $M_L$  and  $M_M$ , 306 K for  $M_E$ , and 318 K for  $P_N$  and  $T_N$ ), along with the nine simulations initiated from a LC structure and carried out at the highest temperature considered (338 K). For these two sets of simulations, the starting phase is the one thermodynamically stable at the given temperature, so that no phase transition is observed. In addition, one of the three simulations involving a transition to the ID phase,  $M_M F_{LC} 302$ , is also included as an example, resulting in 19 main simulations. Illustrative examples involving other simulations are also provided whenever appropriate, and the corresponding detailed results can be found in the Suppl. Mat. document.

The average values of key properties calculated over the last 24 ns of the 19 main simulations are reported in Table 3 (average tilt-angle values; see also Figs. 4 and 5 for illustrative time series as well as Fig. 6 for correlations with the area per lipid), Table 4 (average dihedral-angle *trans* populations; see also Fig. 7 for illustrative time series as well as Fig. 8 for correlations with the

**Table 3**

Average tilt-angle values calculated from a subset of simulations corresponding to equilibrium conditions. This subset encompasses the simulations started from a structure appropriate for the GL phase at reference temperature  $T=302$  (systems  $M_I$  and  $M_M$ ), 306 (system  $M_E$ ) or 318 K (all other systems), as well as from a structure appropriate for the LC phase at reference temperature  $T=338$  K, for the different CSLs (P, T or M), numbers of CSL molecules (N, L, M or E) and hydration levels (F, H or Q). As an example for the ID phase, values for the simulation  $M_M F_{LC} 302$  are also provided (last line). The quantities reported are the final phase of the simulation, the single-lipid apical tilt angle  $\bar{\theta}$  averaged over all lipids and over time, the corresponding root-mean-square deviation  $\sigma_\theta$  over time, the corresponding root-mean-square deviation  $\bar{\gamma}_\theta$  across lipids averaged over time, the collective tilt angle  $\bar{\Theta}$ , and the corresponding root-mean-square deviation  $\sigma_\Theta$  over time, calculated based on the last 24 ns of the simulations. The percentage  $\rho_{GL}$  of configurations in the GL phase over the entire 600 ns simulation time and, when  $\rho_{GL} \geq 10\%$ , the percentage of these GL configurations with the collective azimuthal tilt angles  $\Phi_{bot}$  and  $\Phi_{top}$  for the bottom and top leaflets, respectively, belonging to the specific intervals ( $\pm 15^\circ$  for the bottom layer, within a range of  $15^\circ, \pm 120^\circ$  or  $\pm 60^\circ$  for the top layer, within a range of  $30^\circ$ ) are also reported. The simulation labels and conditions are summarized in Table 1. The data for the entire set of simulations can be found in Tables S.1–S.3 of the Suppl. Mat. document.

Simulation	Final phase	$\bar{\theta}$ [°]	$\sigma_\theta$ [°]	$\bar{\gamma}_\theta$ [°]	$\bar{\Theta}$ [°]	$\sigma_\Theta$ [°]	$\rho_{GL}$ [%]	$P_{+15}^{bot}$ [%]	$P_{-15}^{bot}$ [%]	$P_{+60}^{top}$ [%]	$P_{-60}^{top}$ [%]	$P_{+120}^{top}$ [%]	$P_{-120}^{top}$ [%]	$P_{-60}^{top}$ [%]
$P_N F_{GL} 318$	GL	20.5	4.7	11.8	15.0	8.8	100.0	0.6	98.9	5.4	38.0	13.4	38.3	
$P_N F_{LC} 338$	LC	32.4	2.5	18.8	7.0	3.9	0.0							
$P_N H_{GL} 318$	GL	25.3	1.6	7.0	24.3	1.8	100.0	0.6	99.1	2.4	96.8	0.0	0.7	
$P_N H_{LC} 338$	LC	34.1	3.0	19.2	7.0	3.6	0.0							
$P_N Q_{GL} 318$	GL	25.0	1.8	6.7	24.1	1.9	100.0	0.5	99.3	0.4	99.6	0.0	0.0	
$P_N Q_{LC} 338$	LC	34.9	2.9	19.4	6.7	3.5	0.0							
$T_N F_{GL} 318$	GL	22.3	2.7	10.1	19.8	4.3	100.0	0.5	99.1	5.1	71.5	3.0	16.4	
$T_N F_{LC} 338$	LC	35.1	2.7	19.9	7.2	3.5	0.0							
$T_N H_{GL} 318$	GL	23.0	1.9	9.4	20.7	3.4	100.0	0.5	99.3	2.6	82.0	0.6	11.3	
$T_N H_{LC} 338$	LC	36.5	2.8	20.8	7.9	3.6	0.0							
$T_N Q_{GL} 318$	GL	21.2	2.6	9.0	19.2	3.5	100.0	0.7	99.0	1.9	97.3	0.0	0.0	
$T_N Q_{LC} 338$	LC	38.7	3.0	21.3	8.4	4.5	0.0							
$M_L F_{GL} 302$	GL	22.5	2.2	8.4	20.9	2.5	100.0	0.1	98.9	0.2	52.5	1.7	45.1	
$M_L F_{LC} 338$	LC	37.5	3.8	20.8	6.8	3.7	0.0							
$M_M F_{GL} 302$	GL	20.9	4.0	11.2	14.8	9.5	100.0	30.0	59.6	99.1	0.7	0.0	0.0	
$M_M F_{LC} 338$	LC	39.6	3.1	21.9	7.6	3.8	0.0							
$M_E F_{GL} 306$	GL	23.3	2.7	15.7	16.7	6.0	100.0	4.5	58.9	0.7	99.0	0.0	0.0	
$M_E F_{LC} 338$	LC	43.4	4.2	23.7	8.3	4.5	0.0							
$M_M F_{LC} 302$	ID	10.5	2.3	15.4	4.1	2.2	0.0							

order parameters) and Table 5 (lipid-flipping event statistics; see also Fig. 9 for illustrative time series). The corresponding averages for the entire set of 83 simulations can be found in Suppl. Mat. Tables S.1–S.3, S.4–S.6 and S.7–S.9, respectively.

**Table 4**

Dihedral-angle *trans* populations for selected dihedral angles calculated from a subset of simulations corresponding to equilibrium conditions. This subset encompasses the simulations started from a structure appropriate for the GL phase at reference temperature  $T=302$  (systems  $M_I$  and  $M_M$ ), 306 (system  $M_E$ ) or 318 K (all other systems), as well as from a structure appropriate for the LC phase at reference temperature  $T=338$  K, for the different CSLs (P, T or M), numbers of CSL molecules (N, L, M or E) and hydration levels (F, H or Q). As an example for the ID phase, values for the simulation  $M_M F_{LC} 302$  are also provided (last line). The quantities reported are the final phase of the simulation and the average populations  $\alpha_k$  of *trans* conformations (dihedral angle between  $120^\circ$  and  $240^\circ$ ) for dihedral angle  $\omega_k$ . The dihedral angle  $\omega_k$  is defined by atoms  $C_{k+9}–C_{k+10}–C_{k+11}–C_{k+12}$  according to the numbering of Fig. 1, except  $\omega_1$ , which is defined by  $C_9–C_{11}–C_{12}–C_{13}$ . The data is calculated over the last 24 ns of the simulations and reported here for  $\omega_1, \omega_2, \omega_3$  and  $\omega_{13}$  only. The simulation labels and conditions are summarized in Table 1. The data for the 13 dihedral angles and the entire set of simulations can be found in Tables S.4–S.6 of the Suppl. Mat. document.

Simulation	Final phase	$\alpha_1$ [%]	$\alpha_2$ [%]	$\alpha_3$ [%]	$\alpha_{13}$ [%]
$P_N F_{GL} 318$	GL	91.2	77.3	89.2	71.0
$P_N F_{LC} 338$	LC	84.1	66.6	76.7	63.9
$P_N H_{GL} 318$	GL	92.4	80.3	91.7	72.5
$P_N H_{LC} 338$	LC	83.7	66.2	76.3	63.5
$P_N Q_{GL} 318$	GL	92.6	80.3	91.7	72.2
$P_N Q_{LC} 338$	LC	83.3	66.2	75.7	63.4
$T_N F_{GL} 318$	GL	92.1	79.9	91.0	71.6
$T_N F_{LC} 338$	LC	83.4	66.2	75.7	63.8
$T_N H_{GL} 318$	GL	92.2	80.3	91.3	72.8
$T_N H_{LC} 338$	LC	82.8	66.2	75.2	63.8
$T_N Q_{GL} 318$	GL	92.2	80.5	91.2	71.9
$T_N Q_{LC} 338$	LC	82.7	65.8	74.6	63.5
$M_L F_{GL} 302$	GL	93.9	84.2	93.7	74.7
$M_L F_{LC} 338$	LC	82.8	66.0	75.2	63.8
$M_M F_{GL} 302$	GL	92.5	81.2	91.2	74.3
$M_M F_{LC} 338$	LC	81.9	65.9	74.1	63.3
$M_E F_{GL} 306$	GL	92.5	80.9	91.1	74.2
$M_E F_{LC} 338$	LC	81.1	65.7	73.2	63.2
$M_M F_{LC} 302$	ID	93.2	83.0	93.3	83.4

### 3.2. Tilt angles

Illustrative results for the time evolutions and probability distributions of the different tilt angles over 600 ns are displayed in Figs. 4 and 5 for a subset of simulations. For Fig. 4, these correspond to simulations  $T_N Q_{GL} 322$  (GL phase throughout),  $M_L F_{LC} 338$  (LC phase throughout),  $P_N F_{GL} 322$  (GL → LC transition at about 220 ns) and  $M_E F_{GL} 310$  (GL → LC and LC → ID transitions at about 140 and 500 ns, respectively). For Fig. 5, these correspond to simulations presenting a GL phase throughout, either in the absence or in the presence of MET. Corresponding results for the 19 main simulations are reported in Table 3 in the form of averages over the last 24 ns. The data for the entire set of 83 simulations can also be found in Suppl. Mat. Tables S.1–S.3.

For the three phases, the apical tilt angles  $\theta_n$  of the individual lipids, which characterize the orientation of the lipid head–tail vector relative to the bilayer normal ( $z$ -axis, oriented bottom to top), present relatively narrow distributions around average values characteristic of the phase. The time- and lipid-averaged values  $\bar{\theta}$  of  $\theta_n$  (bottom leaflet) and  $180^\circ – \theta_n$  (top leaflet) are about  $20–25^\circ$  for GL,  $35–45^\circ$  for LC and  $10^\circ$  for ID. The associated time-averaged root-mean-square deviations  $\bar{\gamma}_\theta$  across lipids are about  $5–15^\circ$  for GL,  $20–25^\circ$  for LC and  $15^\circ$  for ID. The collective apical tilt angles  $\Theta_{bot}$  and  $\Theta_{top}$ , which characterize the orientation of the vector sum of the lipid head–tail vectors relative to the bilayer normal, also present narrow distributions around average values characteristic of the phase. The corresponding time- and leaflet-averaged values  $\bar{\Theta}$  of  $\Theta_{bot}$  and  $180^\circ – \Theta_{top}$  are about  $15–25^\circ$  for GL,  $6–8^\circ$  for LC and  $4^\circ$  for ID.

In the GL phase, the individual lipids are thus tilted by  $\bar{\theta}$   $20–25^\circ$  relative to the bilayer normal, this tilt being essentially collective ( $\bar{\Theta} = 15–25^\circ \approx \bar{\theta}$ ). Note in passing that the tilt angle for GMP is somewhat lower than the experimental estimate [93] of  $29.0^\circ$  for the GL phase of DPPC at  $25^\circ C$ , comparable values being found in simulations [94,95]. In the LC phase, the lipids actually present higher tilt angles  $\bar{\theta} \approx 35–45^\circ$  at the individual level. However, this tilt is predominantly non-collective ( $\bar{\Theta} \approx 6–8^\circ \ll \bar{\theta}$ ), i.e. the chains

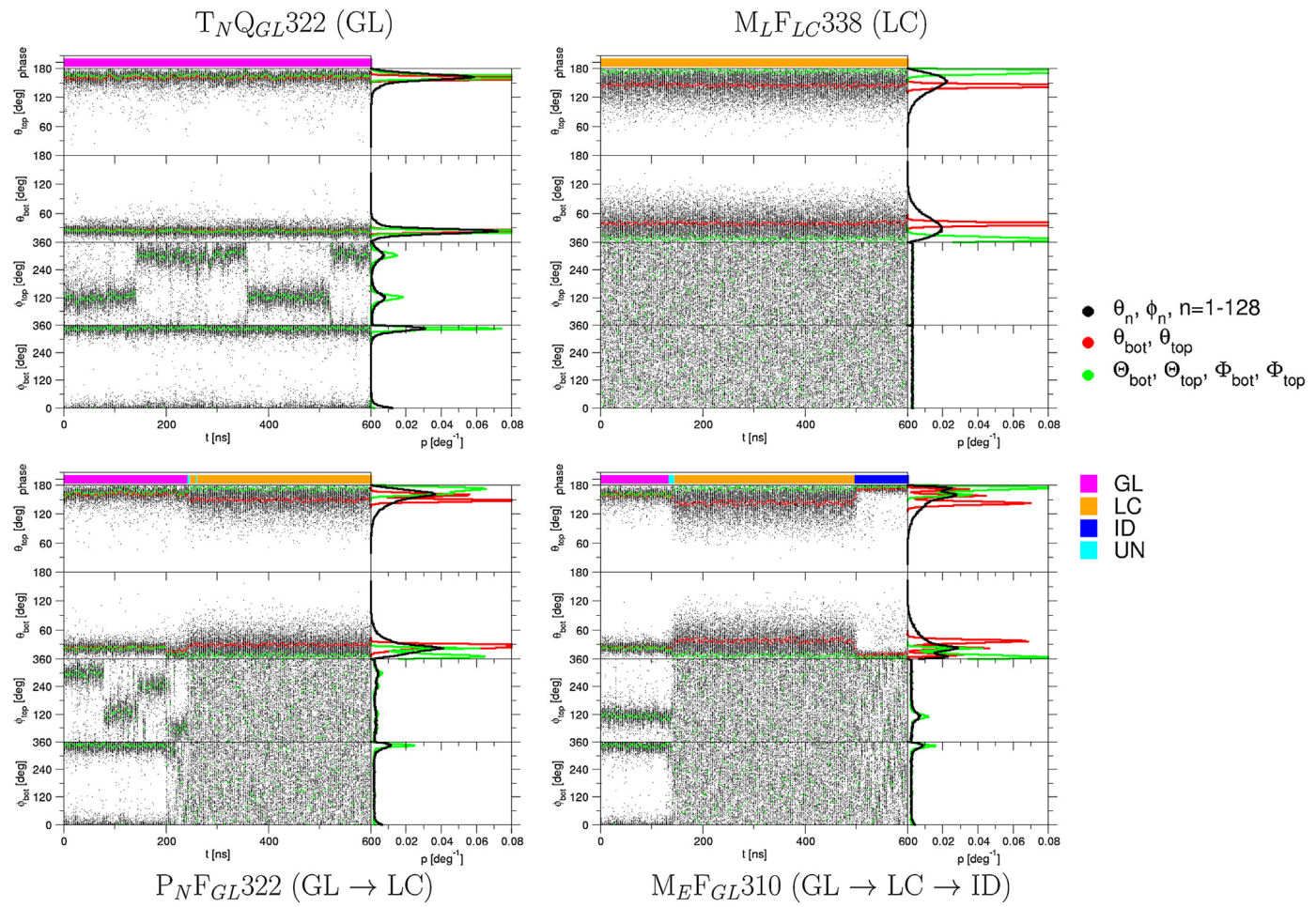


**Fig. 4.** Time series of the tilt angles for a selected subset of simulations presenting different phases. Shown are the phase-assignment descriptor (GL, LC, ID, or UN; color coded bar on top of each panel), the apical ( $\theta_n$ ) and azimuthal ( $\phi_n$ ) tilt-angle values for each individual lipid (black dots), the corresponding lipid-averaged values (apical angle only,  $\theta_{bot}$  and  $\theta_{top}$ ) and the corresponding collective values ( $\Theta_{bot}$  and  $\Theta_{top}$ ,  $\Phi_{bot}$  and  $\Phi_{top}$ ), separately for the bottom and top leaflets over the 600 ns simulation time. The corresponding probability distributions are also shown on the right. The simulation labels and conditions are summarized in Table 1.

**Table 5**  
 Occurrence and timescale of lipid-flipping events calculated from a subset of simulations corresponding to equilibrium conditions. This subset encompasses the simulations started from a structure appropriate for the GL phase at reference temperature  $T = 302$  (systems  $M_L$  and  $M_M$ ), 306 (system  $M_E$ ) or 318 K (all other systems) as well as from a structure appropriate for the LC phase at reference temperature  $T = 338$  K, for the different CSLs (P, T or M), numbers of CSL molecules (N, L, M or E) and hydration levels (F, H or Q). As an example for the ID phase, values for the simulation  $M_M F_{LC} 302$  are also provided (last line). The quantities reported are the final phase, the number of lipids (among 128 simulated) undergoing a special event at least once during the simulation ( $n_{spe}$ ), and for each of the four types of special events (incursion, flip, excursion, hop) the number of events of that type ( $n_{inc}$ ,  $n_{flip}$ ,  $n_{exc}$  and  $n_{hop}$ ), the average time between two events of that type for a single lipid ( $\tau'_{inc}$ ,  $\tau'_{flip}$ ,  $\tau'_{exc}$  and  $\tau'_{hop}$ ; simulation time divided by  $n_{flip}$ ,  $n_{hop}$ ,  $n_{inc}$ , or  $n_{exc}$ , respectively, and by the number of simulated lipids, i.e. 128) and the average duration of one event of that type ( $\tau_{inc}$ ,  $\tau_{flip}$ ,  $\tau_{exc}$  and  $\tau_{hop}$ ). The data is calculated over the entire 600 ns simulations. The simulation labels and conditions are summarized in Table 1. The data for the entire set of simulations can be found in Tables S.7–S.9 of the Suppl. Mat. document.

Simulation	Final phase	$n_{spe}$	$n_{inc}$	$\tau'_{inc}$ [ $\mu$ s]	$\tau_{inc}$ [ns]	$n_{flip}$	$\tau'_{flip}$ [ $\mu$ s]	$\tau_{flip}$ [ns]	$n_{exc}$	$\tau'_{exc}$ [ $\mu$ s]	$\tau_{exc}$ [ns]	$n_{hop}$	$\tau'_{hop}$ [ $\mu$ s]	$\tau_{hop}$ [ns]
P_NF_GL318	GL	1	1	76.80	52.35	0	—	—	0	—	—	0	—	—
P_NF_LC338	LC	16	10	7.68	1.36	3	25.60	1.32	7	10.97	1.54	0	—	—
P_NH_GL318	GL	1	0	—	—	0	—	—	0	—	—	0	—	—
P_NH_LC338	LC	94	23	3.34	1.40	3	25.60	1.76	247	0.31	1.56	8	9.60	1.59
P_NQ_GL318	GL	1	0	—	—	0	—	—	0	—	—	0	—	—
P_NQ_LC338	LC	120	28	2.74	1.59	5	15.36	1.51	616	0.12	1.84	32	2.40	2.25
T_NF_GL318	GL	2	3	25.60	53.01	0	—	—	0	—	—	0	—	—
T_NF_LC338	LC	22	22	3.49	2.61	3	25.60	1.48	0	—	—	0	—	—
T_NH_GL318	GL	3	1	76.80	31.92	0	—	—	0	—	—	0	—	—
T_NH_LC338	LC	33	38	2.02	4.46	6	12.80	4.11	4	19.20	4.78	0	—	—
T_NQ_GL318	GL	1	1	76.80	33.65	0	—	—	0	—	—	0	—	—
T_NQ_LC338	LC	35	46	1.67	10.81	7	10.97	8.50	8	9.60	8.95	0	—	—
M_L F_GL302	GL	3	0	—	—	0	—	—	0	—	—	0	—	—
M_L F_LC338	LC	84	167	0.46	1.33	4	19.20	1.37	74	1.04	1.44	2	38.40	0.72
M_M F_GL302	GL	4	0	—	—	0	—	—	0	—	—	0	—	—
M_M F_LC338	LC	120	467	0.16	1.14	27	2.84	1.59	147	0.52	1.46	10	7.68	2.51
M_E F_GL306	GL	12	8	9.60	51.91	0	—	—	0	—	—	0	—	—
M_E F_LC338	LC	128	2392	0.03	1.29	575	0.13	2.00	425	0.18	1.66	21	3.66	1.89
M_M F_LC302	ID	9	0	—	—	0	—	—	71	1.08	49.01	0	—	—

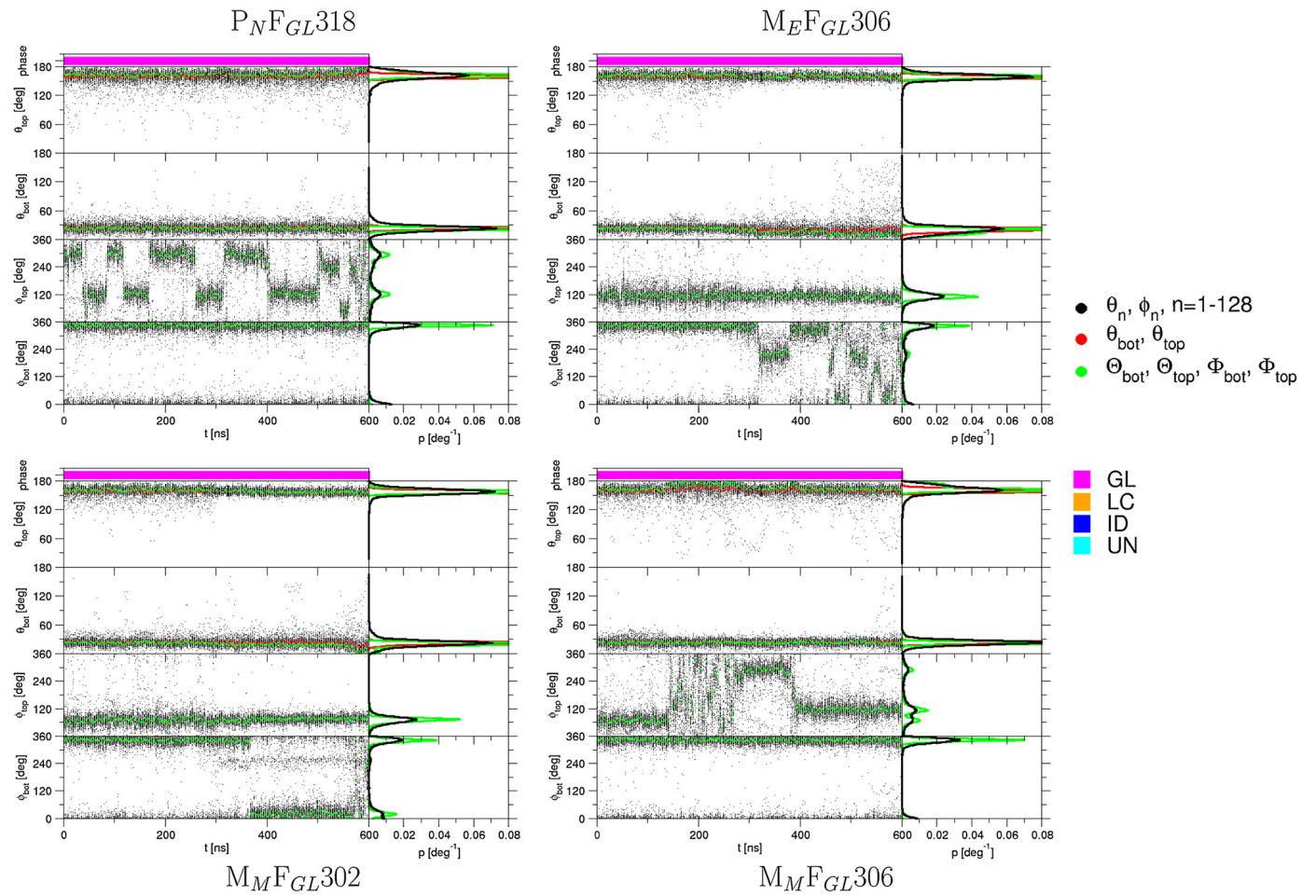


**Fig. 5.** Time series of the tilt angles for a selected subset of simulations in the GL phase. Shown are the phase-assignment descriptor (GL, LC, ID, or UN; color coded bar on top of each panel), the apical ( $\theta_n$ ) and azimuthal ( $\phi_n$ ) tilt-angle values for each individual lipid (black dots), the corresponding lipid-averaged values (apical angle only,  $\theta_{bot}$  and  $\theta_{top}$ ) and the corresponding collective values ( $\Theta_{bot}$  and  $\Theta_{top}$ ,  $\Phi_{bot}$  and  $\Phi_{top}$ ), separately for the bottom and top leaflets over the 600 ns simulation time. The corresponding distributions are also shown on the right. The simulation labels and conditions are summarized in Table 1.

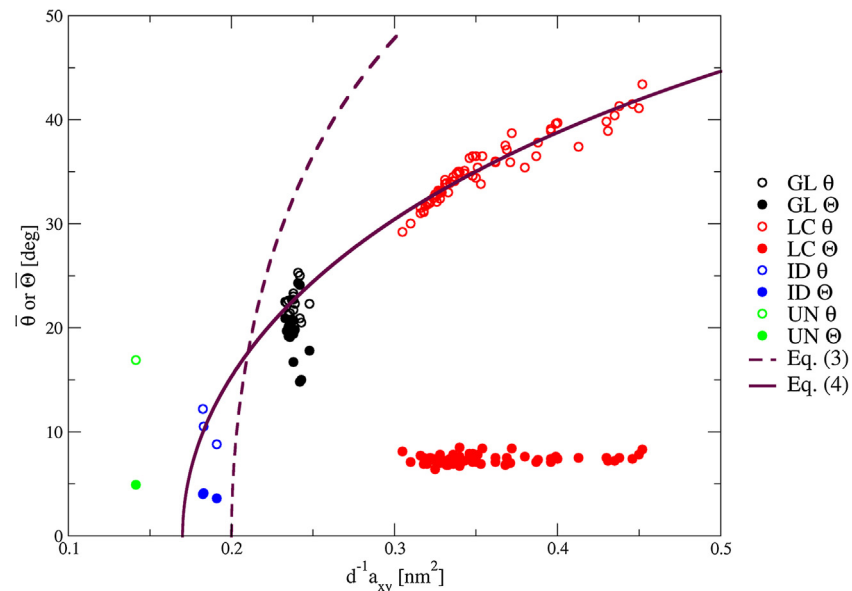


**Fig. 6.** Correlation between the area per lipid and the apical tilt angles. Shown are the average single-lipid ( $\bar{\theta}$ ) and collective ( $\bar{\Theta}$ ) apical tilt angles as a function of the average area per lipid  $a_{xy}$  divided by  $d$  ( $d=1$  for GL and LC,  $d=2$  for ID) for all simulations. The data is averaged over the last 24 ns of the simulations. The curves defined by Eq. (3) with  $s=0.20 \text{ nm}^2$  and Eq. (4) with  $\alpha=1.23 \text{ nm}^{-2}$  and  $s_0=0.17 \text{ nm}^2$  are also shown for comparison. The data is sorted according to the different final phases of the simulations (GL, LC, ID or UN).

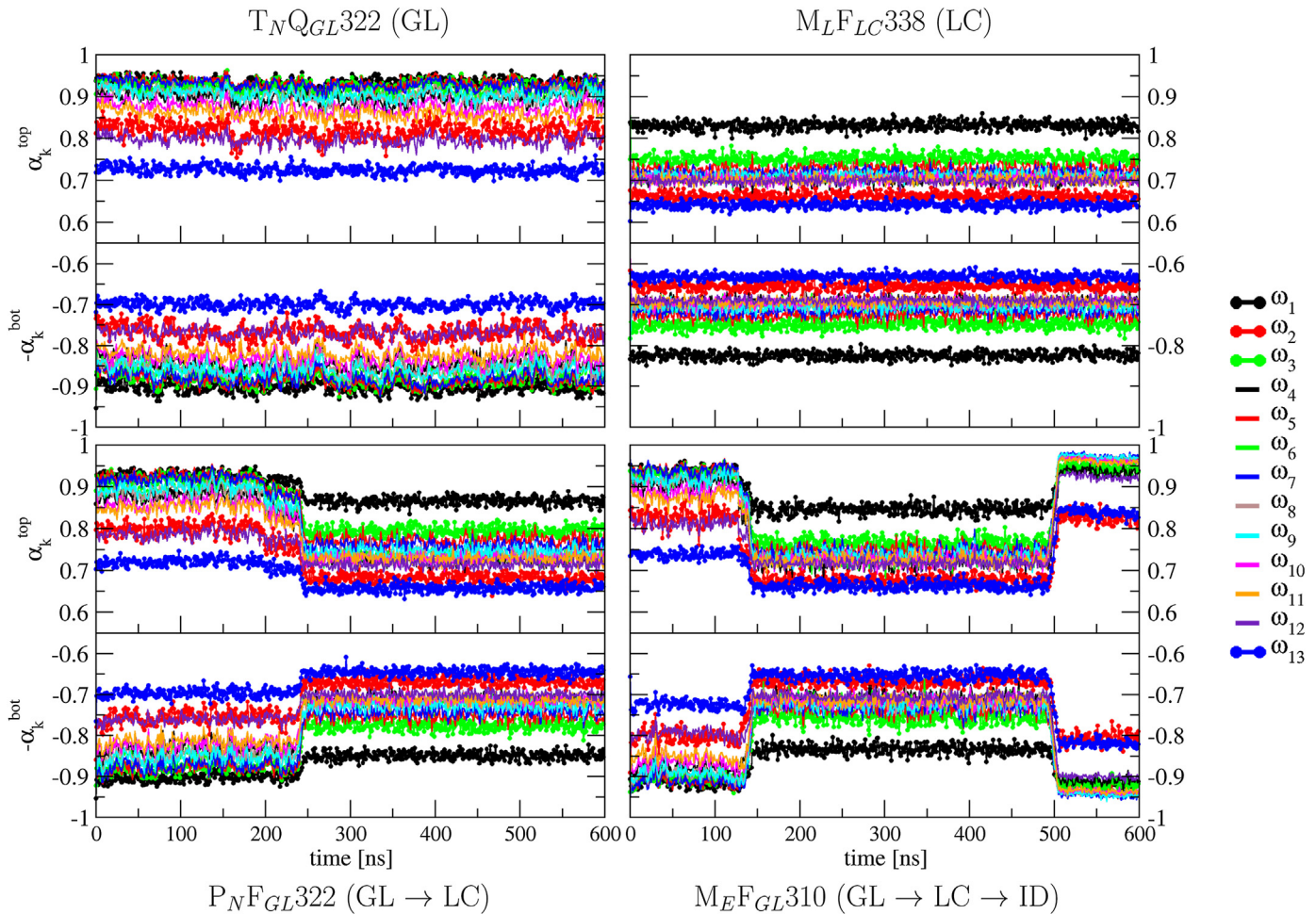


**Fig. 7.** Time series of the dihedral-angle *trans* populations for a selected subset of simulations. Shown are the *trans* populations  $\alpha_n$  of the 13 dihedral angles  $\omega_k$  of the aliphatic tails, separately for the bottom ( $\alpha_k^{bot}$ ) and top ( $\alpha_k^{top}$ ) leaflets, over the 600 ns simulation time. The dihedral angle  $\omega_k$  is defined by atoms  $C_{k+9} - C_{k+10} - C_{k+11} - C_{k+12}$  according to the numbering of Fig. 1, except  $\omega_1$ , which is defined by  $C_9 - C_{11} - C_{12} - C_{13}$ . Note that for the bottom leaflet, the negative value  $-\alpha_k^{bot}$  is reported instead of  $\alpha_k^{bot}$ . The simulation labels and conditions are summarized in Table 1.

tilt in uncorrelated directions. Note that in the context of chains that are not predominantly in all-*trans* conformations, the occurrence of kinks also contributes to an apparent tilt of the head-tail vector [29], i.e. to  $\theta$ . In the ID phase, the chains are only very slightly tilted by  $\bar{\theta} \approx 10^\circ$  at the individual level, the tilt also being essentially non-collective ( $\bar{\Theta} \approx 4^\circ < \bar{\theta}$ ).

These observations concerning the collective nature of the tilt in the GL phase and its non-collective nature in the LC and ID phases are further supported by the analysis of the azimuthal tilt angles  $\phi_n$  of the individual lipids, which characterize the orientation of the lipid head-tail vectors relative to one of the transverse directions (x-axis). As visible in Fig. 4, these angles are essentially randomly distributed in the LC and ID phases. In the GL phase, however, the tilting of the lipids is collective and the distributions of the azimuthal tilt angles  $\phi_n$  define one or more peaks with typical widths of about  $20^\circ$  (see Figs. 4 and 5). These peaks coincide with corresponding peaks in the distributions of the collective azimuthal tilt angles  $\Phi_{bot}$  and  $\Phi_{top}$ , respectively. Interestingly, however, the two leaflets of the bilayer in the GL phase do not present the same preferential values of  $\Phi$ .

The bottom leaflet is nearly always characterized by a value  $\Phi_{bot}$  of about  $-15^\circ$  or, exceptionally,  $+15^\circ$ . The top leaflet generally presents values more or less rapidly oscillating between  $\Phi_{top}$  states at about  $+120$  and  $-60^\circ$  or, less commonly  $+60$  and  $-120^\circ$ . The preference of one leaflet for an azimuthal tilt angle of  $\pm 15^\circ$ , i.e.

for a tilting essentially along an edge of the computational box, is almost certainly an artifact of the *xy*-plane anisotropy associated with the use of periodic boundary conditions in the simulated system. Because the two leaflets of the bilayer are racemic mixtures of the R and S enantiomers of GMP, there is no topological distinction between the bottom and top leaflets, as well as between  $\Phi$  and  $-\Phi$  values. In other words, the observations that the bottom layer (and not the top one) is tilted in a direction close to that of the x-axis and that  $\Phi_{bot}$  is generally about  $-15^\circ$  (more often than  $+15^\circ$ ) are coincidental, i.e. related to the arbitrary initial configuration and the finite sampling time of the simulations. A similar consideration applies to the preference for the x- rather than the y-axis.

In principle, one would expect the top leaflet to be affected by the same type of periodicity-induced preference. However, the relative orientation of the tilt directions of the two leaflets appears to be associated with a stronger driving force, resulting in preferred values of about  $+120$  or  $-60^\circ$  for the relative tilt angle  $\Delta\Phi = \Phi_{top} - \Phi_{bot} \approx \Phi_{top}$ . Here also, due to the racemic nature of the two leaflets, there is no topological distinction between  $+120$  or  $-60^\circ$  and  $-120$  or  $+60^\circ$ . Indeed, the latter values are also observed, their smaller occurrences being again coincidental. The two (or four) preferred states for the relative tilting directions are in slow interconversion, i.e. the simulations evidence precession motions in  $\Delta\Phi$  on a timescale of the order of 50–100 ns with transition durations of about 5–10 ns (see Figs. 4 and 5). Similar changes in

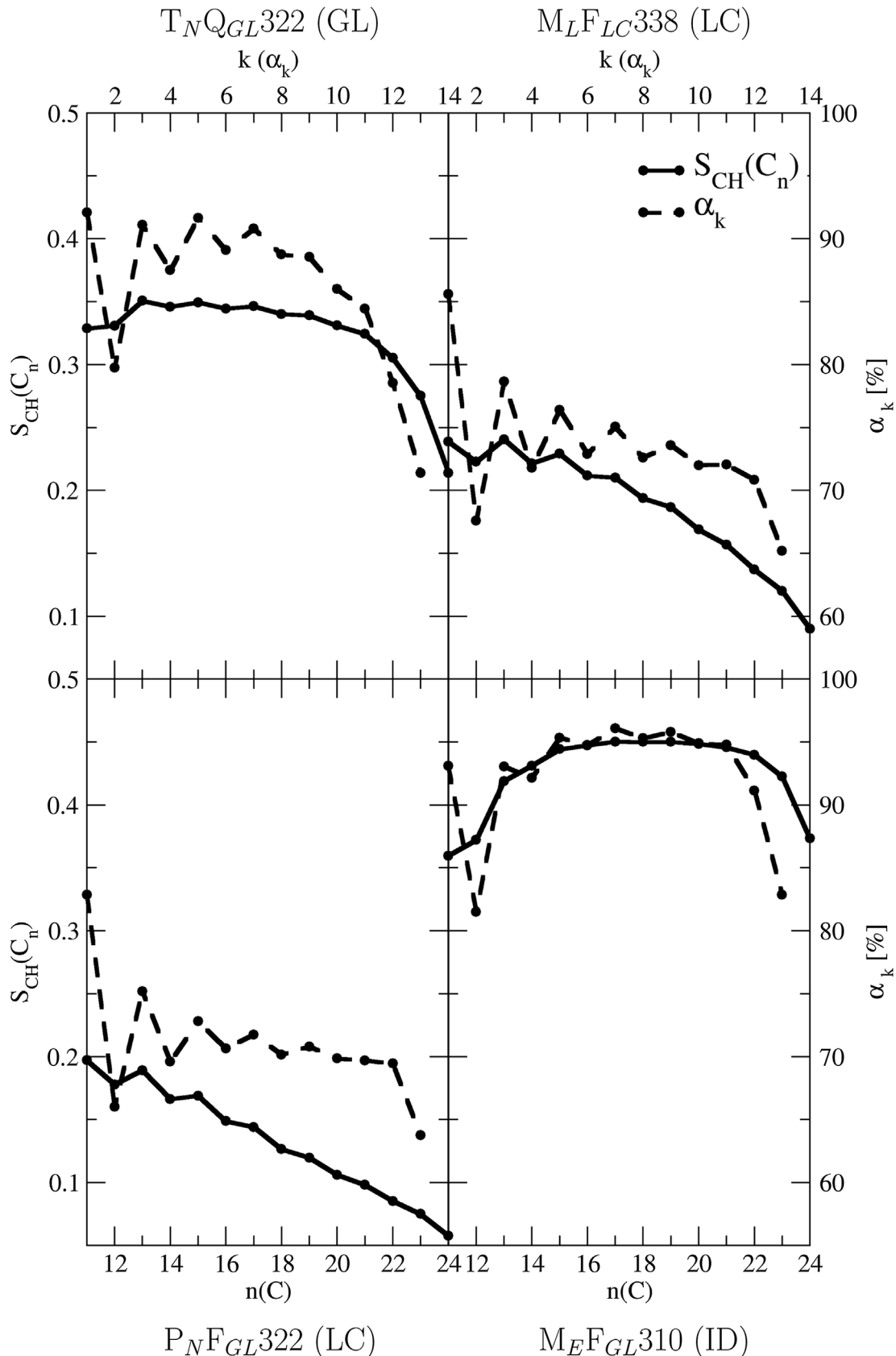


**Fig. 8.** Carbon–hydrogen order parameters and dihedral-angle *trans* populations for a subset of simulations. Shown are the order parameter values  $S_{CH}(C_n)$  for the 14 methylene groups  $n(C)$  in the aliphatic chain ( $n$  following the numbering of Fig. 1) and the *trans* populations  $\alpha_k$  for the 13 dihedral angles  $k$  in the chain. The dihedral angle  $\omega_k$  is defined by atoms  $C_{k+9}–C_{k+10}–C_{k+11}–C_{k+12}$  according to the numbering of Fig. 1, except  $\omega_1$ , which is defined by  $C_9–C_{11}–C_{12}–C_{13}$ . The relation between  $n$  and  $k$  is given by  $k = n - 10$ . The data is averaged over the last 24 ns of the simulations. The simulation labels and conditions are summarized in Table 1. Note that the order parameter graphs shown in Ref. [43] (see Fig. 5 therein) and Ref. [49] (see Fig. 4 therein) were affected by a small calculation error, leading to an erroneous (too low)  $S_{CH}(C_2)$  (numbered 11 in Ref. [49]). This mistake was corrected in Ref. [19] (see Fig. 9 therein).

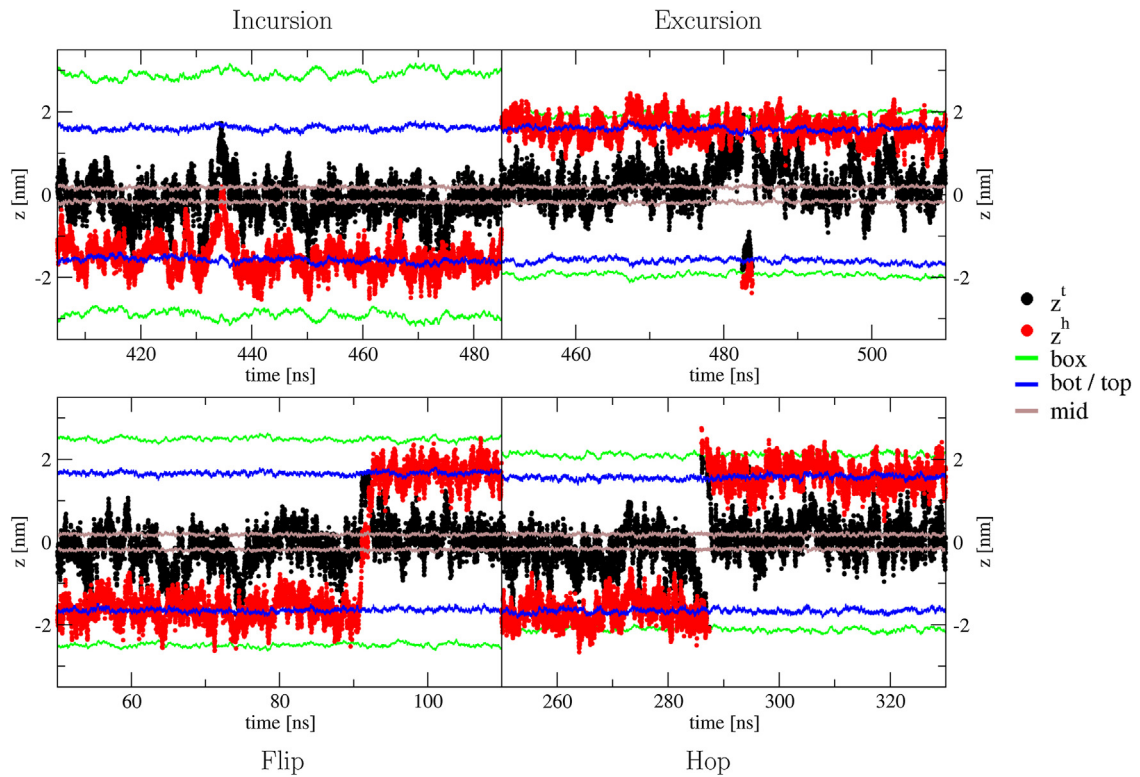


**Fig. 9.** Examples of occurrences of the four types of lipid-flipping events monitored. Shown are segments of lipid trajectories for selected systems illustrating the four types of events monitored (see Eqs. (1) and (2)): incursion (from  $T_{NFlc}338$ ), flip (from  $P_{NFlc}338$ ), excursion (from  $P_{NQlc}338$ ) and hop (from  $P_{NHlc}338$ ). The events are illustrated by time series of the head position  $z^h$  and tail position  $z^t$  of a selected lipid in comparison with the upper and lower leaflet boundaries, box boundaries and tail methyl planes. See Fig. 3c for the definition of the events. The simulation labels and conditions are summarized in Table 1.

azimuthal tilt angles have been observed previously in atomic force microscopy experiments and coarse-grained simulations of DPPC in the GL phase [96]. To our knowledge, however, it is the first time such a precession motion is reported in atomistic MD simulations.

The average angles  $\bar{\theta}$  and  $\bar{\Theta}$  are displayed as a function of the area per lipid  $a_{xy}$  (or its half for the ID phase) in Fig. 6, based on the last 24 ns for the entire set of 83 simulations (see also Fig. 7 in Ref. [19] for corresponding correlations involving other structural properties). Assuming an optimal-packing rigid-rod model of the lipids, the single-lipid apical tilt angle should approximately obey a relationship of the form

$$\cos^{-1} \bar{\theta} = \frac{a_{xy}}{d \cdot s} \quad (3)$$

where  $d=1$  for GL and LC, or  $d=2$  for ID, and  $s$  is the effective tail cross-section. Eq. (3) follows from the idea that a cut at an angle  $\theta+90^\circ$  relative to the axis of a cylinder of section  $s$  exposes a surface of area  $s \cos^{-1} \theta$ . In other words, if a leaflet is modeled as an assembly of  $N$  tightly packed cylinders tilted at an angle  $\theta$  relative to the bilayer normal, the total headgroup area  $N \cdot a_{xy}$  in the  $xy$ -plane increases above  $N \cdot s$  when  $\theta$  increases above  $0^\circ$ , permitting to relieve a possible mismatch between headgroup and tail cross-sections ( $a_{xy} > s$ ). The factor  $d=2$  for the ID phase corresponds to modeling the interdigitated bilayer as an assembly of  $2N$  tightly packed cylinders, which doubles the effect of  $\theta$  on  $a_{xy}$ . Obviously, an optimal-packing rigid-rod model is not expected to be very accurate for the LC phase. Nevertheless, if one assumes that single-lipid tilting dominates over bending (kinking) and that the extent of tail disorder (uncorrelated tilting orientations) does not alter dramatically the chain packing density [19], this model can still be expected to provide a reasonable approximation.

The relationship of Eq. (3) is also displayed in Fig. 6, assuming a value  $s=0.20 \text{ nm}^2$  for the effective cross-section of an alkane chain

[97] based on the lattice parameters of  $n$ -alkane crystals at room temperature. It can be seen that the model is qualitatively correct (trend) but by no means quantitative. Possible reasons for discrepancies include force-field inaccuracies (e.g. too high packing density for the ID phase), suboptimal packing (lowered packing densities for the GL and LC phases), the rather approximate nature of the model for the LC phase (see above), and the different simulation temperatures (increasing in the order ID < GL < LC). Empirically, the data is better reproduced by a function of the form

$$\cos^{-1} \bar{\theta} = 1 + \alpha \left( \frac{a_{xy}}{d} - s_0 \right), \quad (4)$$

also displayed in Fig. 6 with the fitted parameters  $\alpha = 1.23 \text{ nm}^{-2}$  and  $s_0 = 0.17 \text{ nm}^2$ .

### 3.3. Dihedral-angle conformations

Illustrative results for the time evolutions of the average *trans* populations  $\alpha_k^{bot}$  and  $\alpha_k^{top}$  of the 13 dihedral angles of GMP over the 600 ns are displayed in Fig. 7 for a subset of simulations, the same subset considered in Fig. 4. Corresponding results for the 19 main simulations are reported in Table 4 in the form of averages over the last 24 ns and over the two leaflets for the populations  $\alpha_1$ ,  $\alpha_2$ ,  $\alpha_3$  and  $\alpha_{13}$ . The data for the entire set of 83 simulations and for all dihedral angles can also be found in Suppl. Mat. Tables S.4–S.6.

For the GL and LC phases, the first tail dihedral angle  $\omega_1$ , which involves the carbonyl carbon atom of the ester group, presents the highest population of *trans* conformers, i.e. about 93% (GL) and 83% (LC). The *trans* population  $\alpha_1$  is also among the highest in the ID phase, about 93%. In contrast, the second tail dihedral angle  $\omega_2$  presents the second to lowest (GL and LC) or lowest (ID) *trans* population, i.e. about 80% (GL), 66% (LC) and 83% (ID). The dihedral angle  $\omega_3$  is also somewhat peculiar, presenting the second to highest *trans*

population in the LC phase, about 75%. The *trans* population of the last dihedral angle  $\omega_{13}$ , involving the terminal methyl group of the chain, is the lowest (GL and LC) or second to lowest (ID), i.e. about 72% (GL), 64% (LC) and 84% (ID). Finally, the *trans* populations  $\alpha_k$  for the intermediate dihedral angles  $\omega_k$  with  $k=4-12$  present intermediate values, with an approximately constant baseline around 85% (GL), 75% (LC) and 95% (ID) superimposed with an alternating even-odd pattern for  $k=4-8$  (see below). Note that an average population on the order of 70% for the LC phase is in good agreement with the value of 69% estimated based on NMR experiments [98] involving DPPC.

Expectedly, the *trans* populations of all dihedral angles decrease (on average by about 10%) during a GL → LC transition and increase (on average by about 20%) upon a LC → ID transition. For both types of transitions, these changes are least pronounced for the dihedral angles  $\omega_1$ ,  $\omega_2$  and  $\omega_{13}$ . The first dihedral angle  $\omega_1$  is most likely inhibited from free rotation due to the adjacent carbonyl group, thus presenting a high *trans* population in all three phases. The second dihedral angle  $\omega_2$  has more freedom and can be viewed as a “hinge”, accommodating changes in the ordering and packing within the bilayer interior with the ordering of the headgroup region, and thus remaining relatively flexible in the three phases. The low values for  $\omega_{13}$  in all three phases is not surprising, since it involves the terminal methyl group of the tails, which can move rather freely in the absence of a consecutive methylene group. Interestingly, the bottom and top leaflets are not entirely symmetrical, the bottom leaflet consistently presenting slightly higher *trans* populations in all 83 simulations. For the GL phase, this may be correlated with the fact that the tilt-precession motion relative to the  $x$ -axis of the box discussed in Section 3.2 affects the top and not the bottom layer. Note, finally the very high and approximately homogeneous *trans* populations of  $\alpha_1$  and  $\alpha_3-\alpha_{12}$  (all at about 95%) in the ID phase, suggesting a very tight crystal-like packing with nearly perfectly straight all-*trans* chains.

The *trans* populations of the successive dihedral angles along the tail are expected to influence the carbon–hydrogen order parameters  $S_{CH}(C_n)$  of the corresponding methylene groups. The comparison of the  $\alpha_k$  values with  $S_{CH}(C_n)$  values calculated from the simulations (procedure described in Ref. [49]) is shown in Fig. 8 for four illustrative systems, the same as considered in Figs. 4 and 7. The analogy associates the dihedral angle  $\omega_k$  with the methylene group  $C_n$  (numbering of Fig. 1) using  $k=n-10$ , i.e. the second of the four methylene groups defining a dihedral angle along the chain (the associated CH vectors being expected to be most sensitive to this dihedral angle assuming that the headgroup is the most mobile part).

Indeed, a strong correlation is observed between  $S_{CH}(C_n)$  and  $\alpha_k$  with  $k=n-10$ , both curves showing the highest values for ID, high values for GL and low values for LC. The values of both parameters show a drop at the last methylene group, due to the higher freedom of the following methyl group, as observed experimentally for the order parameters [53] of DPPC and the *trans* probabilities [99] for other lipids. One notable difference between the two properties is that the order parameters show a systematic decrease along the chain in the LC phase, which is not seen in the dihedral *trans* populations. This is likely due to the fact that the order parameters account both for the effect of chain disorder and for the average relative orientation with respect to the  $z$ -axis [29,100,101], whereas the  $\alpha_k$  values only include the former effect. This observation may also in part explain the higher order parameters for the ID compared to the GL phase, considering that the former phase is essentially exempt of tilt. However, the very high *trans* populations for ID still suggest a significant contribution of chain ordering.

Another prominent feature in Fig. 8 is the zig–zag pattern of the *trans* populations, alternating a high value for  $\alpha_k$  with a low value for  $\alpha_{k+1}$  (starting with  $k=1$ ), most pronounced for carbon

atoms close to the headgroup and for the GL and LC phases. A similar zig–zag pattern is also observed in terms of the *trans-gauche* isomerization timescales, with higher transition frequencies for the dihedral angles with low *trans* populations (data not shown), the intervals separating isomerization events typically ranging from 100 to 250 ps for the different dihedral angles. This alternating pattern is also visible in the  $S_{CH}(C_n)$  curves for these two phases, most pronounced for the LC phase. A similar pattern has been reported as the odd–even effect in the context of carbon order parameters  $S_{CC}$  for the DPPC system [29] and for other lipids [99,102]. A decrease of the odd–even effect toward the end of the tail [29], as well as an increase of this effect with increasing temperature [99,102] were also reported. The effect was explained in these studies as predominantly arising from the alternation of bond–vector orientations relative to the bilayer normal in a nearly all-*trans* conformation. However, the present analysis shows that the zig–zag pattern is already present (and even more pronounced) in the conformational preferences of the successive dihedral angles along the chain, independently of the bond orientations relative to the  $z$ -axis (dihedral angles are internal coordinates, thus independent of the overall orientation of the lipid molecule). This alternation in the dihedral-angle preferences can itself be explained as a “cascade” effect. Starting from a relatively *trans*-restrained dihedral-angle  $\omega_1$  (proximity of the carbonyl group), the successive angles show in turn flexibility (because the previous angle is *trans*-restrained, relieving the steric pressure on the *gauche* conformations) and rigidity (because the previous angle is flexible, increasing the steric pressure on the *gauche* conformations). This cascade effect is damped along the chain, the terminal dihedral angle  $\omega_{13}$  being itself anomalously flexible (because followed by a methyl group instead of a chain continuation).

### 3.4. Lipid-flipping events

Illustrative situations for the four different types of lipid-flipping events considered here, namely incursions, flips, excursions and hops, are presented in Fig. 9. The statistics of such events over the 19 main simulations are reported in Table 5. The results for the entire set of 83 simulations can be found in Suppl. Mat. Tables S.7–S.9. The event occurrence timescales  $\tau'$ , reported on a per lipid basis, correspond to average times separating two events of a given type in the life of a single lipid. The event durations  $\tau$  are averaged over all the occurring events of the given type, and correspond to the times from the onset to the completion of the event. Note that the statistics concerns the entire 600 ns of the simulations. If the simulation involves a phase transition (Table 2), the results may be ambiguous because they intermingle characteristics of both visited phases. The main simulations considered in Table 5 sample only one phase (except  $M_MFLC302$  with 94% ID phase), and are therefore used as principal source for the following discussion.

The four types of events are relatively infrequent, being separated for a single lipid by intervals on the  $\mu$ s timescale (approximate range 1–100  $\mu$ s; exceptionally down to 30 ns in the presence of MET). In contrast, they are very fast, with durations typically on the ns timescale (approximate range 1–50 ns). The parameters  $\tau$  and  $\tau'$  depend on the dominant phase during the simulation, on the extent of hydration and on the possible presence of CSLs. The incomplete events (incursion and excursion) appear more often than the complete events (flip and hop), consistent with the behavior of phospholipids at bilayer edges [103]. It is important to stress that incursions are only defined by the passage of a headgroup in the bilayer midplane (irrespective of the tail position) and excursions by the passage of a tail methyl group at the box wall in the aqueous region (irrespective of the headgroup position). In particular, excursions often involve a lipid with its headgroup still in the headgroup plane of a leaflet, but its tail transiently pointing into

the aqueous phase. In contrast, hop events typically require the complete transfer of a lipid into the aqueous phase.

In the GL and ID phases, lipid-flipping events are exceptional. Considering the 19 main simulations, a few incursions are observed in the GL phase, and none of the other events. These incursions are infrequent (20–100 μs) but long-lasting (10–50 ns). A number of excursions are observed for the ID phase, and none of the other events. These excursions are more frequent (1 μs) and also long-lasting (50 ns). The scarcity of lipid-flipping events in these two phases, the long duration of the events, and the preference for reinsertion into the same leaflet are easily understood considering the organized tail packing within the bilayer. The preference for incursions in the GL phase and excursions in the ID phase may be related to the intrinsic packing deficit (resulting in tilting) in the former phase and the packing excess (doubling of the number of tails in the bilayer plane) in the latter phase. The influence of MET, which reduces the polarity of the aqueous phase, may also explain why excursions are facilitated in the ID phase.

In contrast, lipid-flipping events are relatively frequent in the LC phase. Incursions and excursions are the most frequent events. Their durations are in the range 1–10 ns, with little influence of the environment. The average time separating these events is typically about 1–20 μs in the absence of MET. However it decreases to 30–180 ns in the presence of MET at the highest concentration. This is certainly related to the increased bilayer fluidity and the lower polarity of the aqueous phase. The average time separating incursions slightly decreases upon decreasing the hydration in the absence of TRH, whereas it increases in the presence of this CSL. The average time separating excursions rapidly decreases upon decreasing the hydration level in the absence of TRH. This is certainly related to the closer periodic stacking of the bilayer (reduced thickness of the aqueous phase). However, TRH largely reduces the frequency of these events at all hydration levels, presumably due to the formation of a surface coating layer.

Flip events in the LC phase have durations in the range 1–10 ns, with little influence of the environment. The average time separating these events is typically about 10–20 μs in the absence of MET. However it decreases to 130 ns in the presence of MET at the highest concentration. Dehydration, addition of TRH and, to an even higher extent, addition of MET tend to decrease the interval between these events. The durations of incursion and flip events are lower by one order of magnitude compared to the corresponding estimates for cholesterol migration in a coarse-grained simulation study [94] of DPPC lipid bilayers at 323 K (estimated to 0.3 and 0.6 μs, respectively). Hop events in the LC phase only occur at low hydration (half or quarter; close periodic stacking of the bilayer) in the absence of TRH (formation of a coating layer), or in the presence of MET (increased bilayer fluidity, decreased environment polarity). They have durations of 1–2 ns, with little influence of the environment. The average time separating these events is about 2–10 μs in the absence of MET. In the presence of MET, this time decreases with increasing MET concentration, from 40 to 4 μs.

Although relatively scarce, flip and hop events in the LC phase result in the transfer of a lipid molecule across the two leaflets of the bilayer. They may thus *a priori* generate an imbalance in the number of lipids in each leaflet or, considering that the leaflets are initially racemic, cause an enantiomeric enrichment of the leaflets. This was checked (data not shown) and, besides limited fluctuations, neither of the two processes was observed in the simulations.

#### 4. Conclusion

The aim of the present study was to investigate the occurrence of long-timescale motions in previously reported [19] 600 ns MD simulations of a 2 × 8 × 8 GMP bilayer patch. The results of this study, along with those of the previous work [19,43,48,49,64,65], provide a detailed picture of the motions occurring in GMP bilayers, along with the associated characteristic event durations and occurrence timescales. This picture is summarized in Table 6.

From a broad perspective, the phase properties of lipids result from a balance [9] between hydrophobic effects (tail clustering) and hydration forces (headgroup solvation). However, an equally important factor governing these properties is the usual mismatch between the effective (hydrated) headgroup and the straight (*all-trans*) tail cross-sections, in interplay with the requirement of close packing within the bilayer interior [19]. Typically, the effective headgroup cross-section is larger than the tail cross-section, as well as modulated by the environmental conditions, prominently the hydration level, the concentration of MET, and the temperature (TRH having a comparatively weaker effect).

The following mechanisms may act to reduce the effect of the suboptimal tail packing that would result from a straight orientation of the tails parallel to the bilayer normal [104,105], as illustrated in Fig. 10: (A) introduction of bending (kinking) in the tails, reducing the bilayer thickness and increasing the effective tail cross section relative to *all-trans* conformations [106]; (B) tilting of straight lipid chains, leading to the same result [107]; (C) interdigitation of the lipid chains, resulting in a doubling of the number of tails per *xy*-area element in the bilayer interior; (D) tilting of the glycerol backbone relative to the bilayer surface [108]; and (E) adjustment of the headgroup substituent orientation and packing properties [61]. Mechanisms D and E are irrelevant in the context of GMP, which has a single chain and no headgroup substitution. In this case, mechanisms A, B and C can be viewed as the characteristic mismatch-repair mechanisms for the LC, GL and ID phases, respectively, the occurrence of phase transitions between these phases being viewed as a switch between different mechanisms. The three mechanisms are thus random tilting or kinking of the chains (characterized by the single-lipid tilt angle  $\theta$  and active in the LC phase), collective tilting of the chains in each leaflet (characterized by the collective tilt angle  $\Theta$  and active in the GL phase), and interdigitation (active in the ID phase, and associated with [109] low values of  $\theta$  and  $\Theta$ ). For bilayers consisting of diglycerides or involving a headgroup substituent, tilting of the glycerol backbone (D) or

**Table 6**  
Typical durations and intervals characteristic of motions occurring in GMP lipid bilayers, as inferred from MD simulations. Shown are indicative ranges for the durations and intervals corresponding to different types of motion. The duration refers to the time taken by the event and the interval to the time separating two successive events. The data primarily refers to a pure bilayer in water at full hydration, at 1 bar and close to  $T_m$  (about 315 K). Different environmental conditions (temperature, phase, presence and concentration of CSLs) can alter the indicated timescales. For the phase transitions, the values are representative for a temperature range within 10 K of  $T_m$ . For the tilt precession, shifts  $\Delta\Phi$  in the relative collective tilt angle by 60 or 120° are considered. The typical intervals separating lipid-flipping events are reported on a per lipid basis.

Type	Duration	Interval	Ref.
Translational diffusion	$3\text{--}14 \times 10^{-5} \text{ nm}^2 \text{ ps}^{-1}$	–	Refs. [19,49]
Dihedral-angle isomerization	–	100–250 ps	This work
Single-lipid rotation	0.1–0.2 ns	–	Refs. [19,49]
Single-lipid wobbling	1–10 ns	–	Refs. [19,49]
Phase transitions	2–10 ns	2–10 μs	Refs. [19,43,49]
Tilt precession	5–10 ns	50–100 ns	This work
Lipid flipping	1–50 ns	1–100 μs	This work

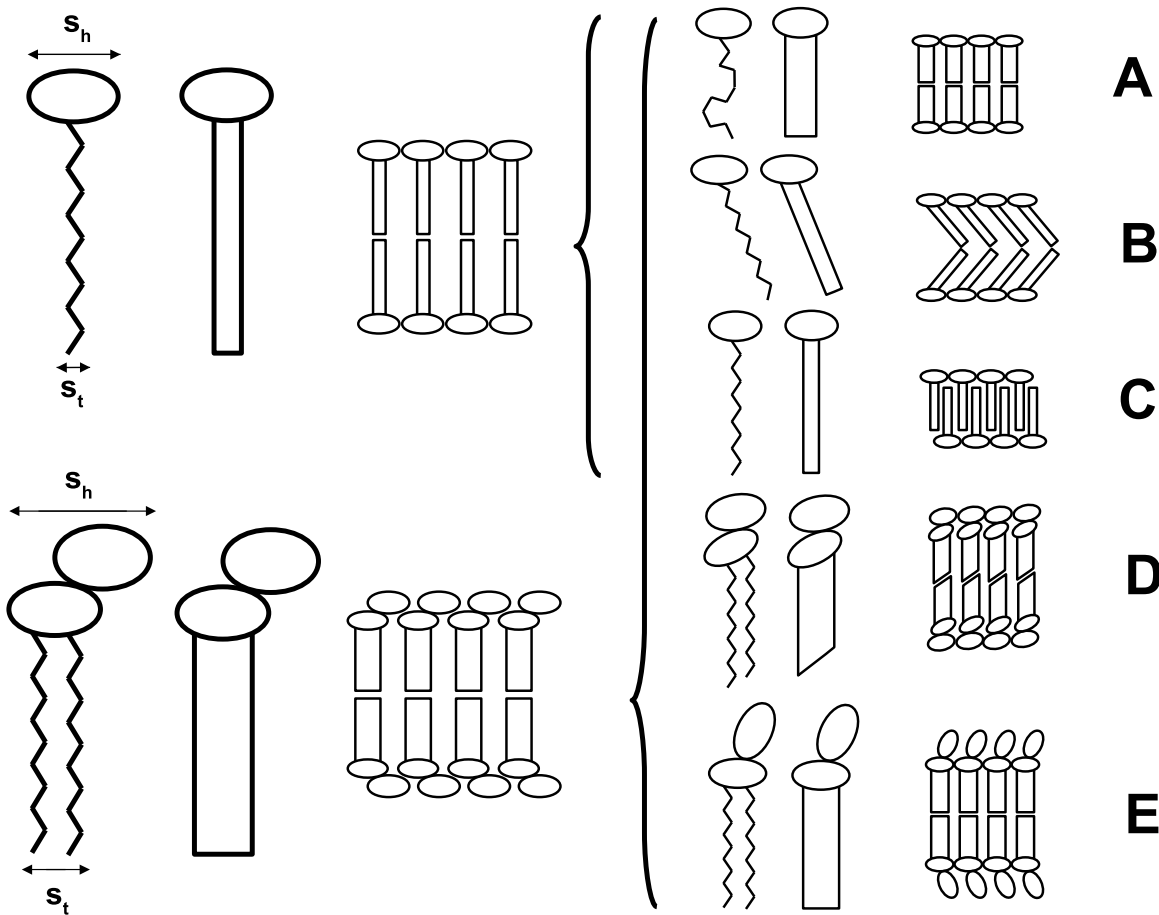


**Fig. 10.** Schematic illustration of five possible mechanisms to relieve a suboptimal tail packing induced by the mismatch between headgroup and tail cross-sections. Mismatch (left) between the effective cross-section  $s_h$  of the (hydrated) headgroups and the effective cross-section  $s_t$  of the tail(s) when all-trans and parallel to the bilayer normal, for a simple monoglyceride (top) or a diglyceride with headgroup substitution (bottom). Possible mechanisms (right) to improve the tail packing, namely: (A) bending (kinking) of the tail; (B) tilting of the all-trans tail (note that the two leaflets need not tilt in the same direction); (C) interdigitation; (D) tilting of the glycerol backbone relative to the headgroup plane; and (E) adjustment of the headgroup orientation and packing properties.

adjustment of the substituent orientation and packing properties (E) represent additional possible mechanisms. The occurrence of ripple phases for DPPC and other lipids can be viewed as a superposition of two types of mechanisms involving alternation of local micro-domains [62,110]. As detailed elsewhere [65], phase transitions in the GMP system are fast and infrequent events, with durations on the order of 2–10 ns but occurrence frequencies in the  $\mu\text{s}$  regime at temperatures close to  $T_m$ .

The occurrence of tilt-precession motions was identified in the GL phase, which is the only one presenting a significant collective tilt of the two leaflets. The preferred relative orientations of the tilting directions correspond to  $\Delta\Phi$  values of  $\pm 60^\circ$  or  $\pm 120^\circ$ . A precession motion between these values occurs on a time scale of about 50–100 ns with transition durations of about 5–10 ns. Since the simulated bilayers involve racemic leaflets, no preference between positive and negative angles is expected, and residual differences arise from the long timescale of the precession relative to the duration of the simulations. Nevertheless, it is interesting to speculate whether bilayers consisting of enantiomerically pure leaflets could evidence a transmission of the single-lipid chirality into a mesoscopic tilt-angle chirality (work is in progress to assess this possibility). This would represent another mechanism of microscopic-to-mesoscopic chirality transmission in lipids, besides that involving enantiomeric segregation and microdomain formation, as observed e.g. experimentally in GMP monolayers [111] and by simulation in GMP bilayers [48]. Note that further simulations

in the presence of MET also revealed similar precession motions in the ID phase, as discussed elsewhere [64].

The dihedral angle *trans* populations are expectedly very high in the ordered and tightly packed GL and ID phases, and comparatively lower for the disordered and fluid LC phase. However, in the three phases, the distribution of the *trans* populations along the chain are far from homogeneous, typically presenting a damped odd-even pattern (starting from a high-*trans* first dihedral involving the carbonyl carbon atom, followed by a low-*trans* “hinge” dihedral, etc.) and ending with a particularly low *trans* populations for the last dihedral (involving the terminal methyl group). These patterns translate into corresponding patterns for the carbon-hydrogen order parameters, where the influence of dihedral-angle ordering is combined with that of the orientation of the successive bonds relative to the bilayer normal, which depends in particular on the extent of tilting of the lipids in a given phase. In this respect, the simulation results suggest that the odd–even alternation in the order parameters, observed experimentally for other lipids, should not be interpreted as solely resulting from an effect of all-*trans* bond orientations relative to the bilayer normal, but also in terms of alternating dihedral-angle conformational preferences.

Finally, four types of lipid-flipping events were monitored, namely incursions, flips, excursions and hops. These events may be of great relevance for various biochemical processes. For example, it has been suggested that an excursion-type event may be at the onset of membrane fusion processes [112] and that lipid flip-flop

may be a crucial step for the formation of pores in certain biological membranes [113]. In GMP, lipid-flipping events represent fast and infrequent events, with durations on the ns timescale, but occurrence intervals (for a single lipid) on the  $\mu$ s timescale. These events are very infrequent in the ordered GL and ID phases (tight chain packing), comparatively more frequent in the more fluid LC phase, and may become very frequent in the presence of MET at high concentrations (increased bilayer fluidity and headgroup spacing, decreased solution polarity). In contrast, TRH reduces the frequency of these motions, entirely suppressing those involving transfer via the aqueous phase (coating layer, H-bonded lipid bridging). Flip and hop events lead to small fluctuations in the number of lipids per leaflet and in their enantiomeric content, but no systematic trend is observed in these properties.

The present study provides a picture of GMP bilayers involving a rich spectrum of events occurring on a wide range of timescales (Table 6), from the 100-ps range isomerization of single dihedral angles, via the 100-ns range of tilt precession motions, to the multi- $\mu$ s range of phase transitions and lipid-flipping events. Although less relevant than DPPC, GMP represents an extraordinary testing ground for the exploration of basic bilayer properties in the context of computationally less expensive MD simulations (thus better converged and easier to repeat under different environmental conditions). Still, the fundamental understanding gained in this context certainly also bears a basic qualitative relevance for more complex, strongly interacting, and slowly relaxing bilayer systems.

## Acknowledgment

Financial support from the Swiss National Foundation (Grants 21-132739 and 21-138020) is gratefully acknowledged.

## Appendix A. Supplementary data

Supplementary data associated with this article can be found, in the online version, at <http://dx.doi.org/10.1016/j.jmgm.2014.10.016>.

## References

- [1] G.M. Cooper, R.E. Hausman, *The Cell: A Molecular Approach*, ASM Press, Washington, DC, USA, 2007.
- [2] K. Kawai, M. Fujita, M. Nakao, Lipid components of the two different regions of an intestinal epithelial cell membrane of mouse, *Biochim. Biophys. Acta* 369 (1974) 222.
- [3] A.A. Spector, M.A. Yorek, Membrane lipid composition and cellular function, *J. Lipid Res.* 26 (1985) 1015.
- [4] P.L. Yeagle, Lipid regulation of cell membrane structure and function, *FASEB J.* 3 (1989) 1833.
- [5] M. Boom, E. Evans, O. Mouritsen, Physical properties of the fluid lipid-bilayer component of cell membranes: a perspective, *Q. Rev. Biophys.* 24 (1991) 293.
- [6] J.M. Seddon, G. Cevc, Lipid polymorphism: structure and stability of lyotropic mesophases of phospholipids, in: G. Cevc (Ed.), *Phospholipids Handbook*, Marcel Dekker, Inc., New York, USA, 1993, pp. 403–454.
- [7] I. Foubert, K. Dewettinck, D. van de Walle, A.J. Dijkstra, P.J. Quinn, Physical properties: structural and physical characteristics, in: F.D. Gunstone, J.L. Harwood, A.J. Dijkstra (Eds.), *The Lipid Handbook*, 3rd edition, CRC Press, Div. of Taylor, Francis Group, Boca Raton, USA, 2007, pp. 471–534.
- [8] J.F. Nagle, S. Tristram-Nagle, Structure of lipid bilayers, *Biochim. Biophys. Acta* 1469 (2000) 159.
- [9] M. Venturoli, M.M. Sperotto, M. Kranenburg, B. Smit, Mesoscopic models of biological membranes, *Phys. Rep.* 437 (2006) 1.
- [10] B.F. Qiao, M. Olvera de la Cruz, Driving force for crystallization of anionic lipid membranes revealed by atomistic simulations, *J. Phys. Chem. B* 117 (2012) 5073.
- [11] K. Ohki, K. Tamura, I. Hatta, Ethanol induces interdigitated gel phase ( $L_{\beta I}$ ) between lamellar gel phase ( $L_{\beta'}$ ) and ripple phase ( $P_{\beta'}$ ) in phosphatidylcholine membranes: a scanning density meter study, *Biochim. Biophys. Acta* 1023 (1990) 215.
- [12] J. Mou, J. Yang, C. Huang, Z. Shao, Alcohol induces interdigitated domains in unilamellar phosphatidylcholine bilayers, *Biochemistry* 33 (1994) 9981.
- [13] L.L. Holte, K. Gawrisch, Determining ethanol distribution in phospholipid multilayers with MAS-NOESY spectra, *Biochemistry* 36 (1997) 4669.
- [14] V. Chupin, J.-W.P. Boots, J.A. Killian, R.A. Demel, B. de Kruijff, Lipid organization and dynamics of the monostearoylglycerol–water system. A  $^2$ H NMR study, *Chem. Phys. Lipids* 109 (2001) 15.
- [15] L.B. Chen, M.L. Johnson, R.L. Biltonen, A macroscopic description of lipid bilayer phase transitions of mixed-chain phosphatidylcholines: chain-length and chain-asymmetry dependence, *Biophys. J.* 80 (2001) 254.
- [16] M. Kranenburg, B. Smit, Phase behavior of model lipid bilayers, *J. Phys. Chem. B* 109 (2005) 6553.
- [17] S. Tristram-Nagle, R. Zhang, R.M. Suter, C.R. Worthington, W.-J. Sun, J.F. Nagle, Measurement of chain tilt angle in fully hydrated bilayers of gel phase lecithin, *Biophys. J.* 64 (1993) 1097.
- [18] Y. Takaoka, M. Paseniewicz-Gierula, H. Miyagawa, K. Kitamura, Y. Tamura, A. Kusumi, Molecular dynamics generation of nonarbitrary membrane models reveals lipid orientational correlations, *Biophys. J.* 79 (2000) 3118.
- [19] M. Laner, B.A.C. Horta, P.H. Hünenberger, Effect of the cosolutes trehalose and methanol on the equilibrium and phase-transition properties of glycerol-monopalmitate lipid bilayers investigated using molecular dynamics simulations, *Eur. Biophys. J.* 43 (2014) 517.
- [20] S.A. Simon, T.J. McIntosh, Interdigitated hydrocarbon chain packing causes the biphasic transition behavior in lipid/alcohol suspensions, *Biochim. Biophys. Acta* 773 (1984) 169.
- [21] J.M. Boggs, G. Rangaraj, Phase transitions and fatty acid spin label behavior in interdigitated lipid phases induced by glycerol and polymyxin, *Biochim. Biophys. Acta* 816 (1985) 221.
- [22] J.-S. Chiou, P.R. Krishna, H. Kamaya, I. Ueda, Alcohols dehydrate lipid membranes: an infrared study on hydrogen bonding, *Biochim. Biophys. Acta* 1110 (1992) 225.
- [23] J.A. Barry, K. Gawrisch, Direct NMR evidence for ethanol binding to the lipid–water interface of phospholipid bilayers, *Biochemistry* 33 (1994) 8082.
- [24] C.-H. Chen, K. Hoye, L.G. Roth, Thermodynamic and fluorescence studies of the underlying factors in benzyl alcohol-induced lipid interdigitated phase, *Arch. Biochem. Biophys.* 333 (1996) 401.
- [25] S.E. Feller, C.A. Brown, D.T. Nizza, K. Gawrisch, Nuclear Overhauser enhancement spectroscopy cross-relaxation rates and ethanol distribution across membranes, *Biophys. J.* 82 (2002) 1396.
- [26] R. Kind, R. Blinc, H. Arend, P. Muralt, J. Slak, G. Chapuis, K.J. Schenk, B. Zeks, Dynamics of the *n*-decylammonium chains in the perovskite-type layer structure compound  $(C_{10}H_{21}NH_3)_2CdCl_4$ , *J. Chem. Phys.* 71 (1979) 2118.
- [27] R. Kind, R. Blinc, H. Arend, P. Muralt, J. Slak, Phase transition from an intercalated to a nonintercalated structure in a lipid bilayer, *Phys. Rev. A* 26 (1982) 1816.
- [28] K.W. Lee, C.H. Lee, J.K. Kang, Low-frequency chain dynamics in decylammonium chloride, *J. Phys. Soc. Jpn.* 70 (2001) 2888.
- [29] J.-P. Douliez, A. Ferrarini, E.-J. Dufourc, On the relationship between C–C and C–D order parameters and its use for studying the conformation of lipid acyl chains in biomembranes, *J. Chem. Phys.* 109 (1998) 2513.
- [30] S.-J. Marrink, O. Berger, P. Tieleman, F. Jähnig, Adhesion forces of lipids in a phospholipid membrane studied by molecular dynamics simulations, *Biophys. J.* 74 (1998) 931.
- [31] E. Lindahl, O. Edholm, Spatial and energetic-entropic decomposition of surface tension in lipid bilayers from molecular dynamics simulations, *J. Chem. Phys.* 113 (2000) 3882.
- [32] B.W. Lee, R. Faller, A.K. Sum, I. Vattulainen, M. Patra, M. Karttunen, Structural effects of small molecules on phospholipid bilayers investigated by molecular simulations, *Fluid Phase Equilib.* 225 (2004) 63.
- [33] C.S. Pereira, R.D. Lins, I. Chandrasekhar, L.C.G. Freitas, P.H. Hünenberger, Interaction of the disaccharide trehalose with a phospholipid bilayer: a molecular dynamics study, *Biophys. J.* 86 (2004) 2273.
- [34] B.W. Lee, R. Faller, A.K. Sum, I. Vattulainen, M. Patra, M. Karttunen, Structural effects of small molecules on phospholipid bilayers investigated by molecular simulations, *Fluid Phase Equilib.* 228 (2005) 135.
- [35] A. Skibinsky, R.M. Venable, R.W. Pastor, A molecular dynamics study of the response of lipid bilayers and monolayers to trehalose, *Biophys. J.* 89 (2005) 4111.
- [36] J. Chanda, S. Bandyopadhyay, Perturbation of phospholipid bilayer properties by ethanol at a high concentration, *Langmuir* 22 (2006) 3775.
- [37] M. Patra, E. Salonen, E. Terama, I. Vattulainen, R. Faller, B.W. Lee, J. Holopainen, M. Karttunen, Under the influence of alcohol: the effect of ethanol and methanol on lipid bilayers, *Biophys. J.* 90 (2006) 1121.
- [38] C.S. Pereira, P.H. Hünenberger, Interaction of the sugars trehalose, maltose and glucose with a phospholipid bilayer: a comparative molecular dynamics study, *J. Phys. Chem. B* 110 (2006) 15572.
- [39] V. Knecht, S.-J. Marrink, Molecular dynamics simulations of lipid vesicle fusion in atomic detail, *Biophys. J.* 92 (2007) 4254.
- [40] J.L. MacCallum, D.P. Tieleman, Interactions between small molecules and lipid bilayers, *Curr. Top. Membr.* 60 (2008) 227.
- [41] C.S. Pereira, P.H. Hünenberger, Effect of trehalose on a phospholipid membrane under mechanical stress, *Biophys. J.* 95 (2008) 3525.
- [42] C.S. Pereira, P.H. Hünenberger, The influence of polyhydroxylated compounds on a hydrated phospholipid bilayer: a molecular dynamics study, *Mol. Simulat.* 34 (2008) 403.
- [43] B.A.C. Horta, A.H. de Vries, P.H. Hünenberger, Simulating the transition between gel and liquid-crystal phases of lipid bilayers: dependence of the transition temperature on the hydration level, *J. Chem. Theor. Comput.* 6 (2010) 2488.

- [44] A.P. Lyubartsev, A.L. Rabinovich, Recent development in computer simulation of lipid bilayers, *Soft Matter* 7 (2011) 25.
- [45] H. Saito, W. Shinoda, Cholesterol effect on water permeability through DPPC and PSM lipid bilayers: a molecular dynamics study, *J. Phys. Chem. B* 115 (2011) 15241.
- [46] E. Yamamoto, T. Akimoto, H. Shimizu, Y. Hirano, M. Yasui, K. Yasuoka, Diffusive nature of xenon anesthetic changes properties of a lipid bilayer: molecular dynamics simulations, *J. Phys. Chem. B* 116 (2012) 8989.
- [47] B.A.C. Horta, L. Perić-Hässler, P.H. Hünenberger, Interaction of the disaccharides trehalose and gentiobiose with lipid bilayers: a comparative molecular dynamics study, *J. Mol. Graph. Model.* 29 (2010) 331.
- [48] B.A.C. Horta, P.H. Hünenberger, Enantiomeric segregation in the gel phase of lipid bilayers, *J. Am. Chem. Soc.* 133 (2011) 8464.
- [49] M. Laner, B.A.C. Horta, P.H. Hünenberger, Phase-transition properties of glycerol-monopalmitate lipid bilayers investigated by molecular dynamics simulation: influence of the system size and force-field parameters, *Mol. Simulat.* 39 (2013) 563.
- [50] C. Anézo, A.H. de Vries, H.-D. Höltje, D.P. Tielemans, S.-J. Marrink, Methodological issues in lipid bilayer simulations, *J. Phys. Chem. B* 107 (2003) 9424.
- [51] J.B. Klauda, R.M. Venable, A.D. MacKerell Jr., R.W. Pastor, Considerations for lipid force field development, *Curr. Top. Membr.* 60 (2008) 1.
- [52] D.P. Tielemans, B. Hess, M.S.P. Sansom, Analysis and evaluation of channel models: simulation of alamethicin, *Biophys. J.* 83 (2002) 2393.
- [53] M. Patra, M. Karttunen, M.T. Hyvönen, E. Falck, P. Lindqvist, I. Vattulainen, Molecular dynamics simulations of lipid bilayers: major artifacts due to truncating electrostatic interactions, *Biophys. J.* 84 (2003) 3636.
- [54] M. Patra, M. Karttunen, M.T. Hyvönen, E. Falck, I. Vattulainen, Lipid bilayers driven to a wrong lane in molecular dynamics simulations by subtle changes in long-range electrostatic interactions, *J. Phys. Chem. B* 108 (2004) 4485.
- [55] M.A. Kastenholz, P.H. Hünenberger, Influence of artificial periodicity and ionic strength in molecular dynamics simulations of charged biomolecules employing lattice-sum methods, *J. Phys. Chem. B* 108 (2004) 774.
- [56] A. Cordomí, O. Edholm, J. Perez, Effect of different treatments of long-range interactions and sampling conditions in molecular dynamic simulations of rhodopsin embedded in a dipalmitoyl phosphatidylcholine bilayer, *J. Comput. Chem.* 28 (2007) 1017.
- [57] M.M. Reif, V. Kräutler, M.A. Kastenholz, X. Daura, P.H. Hünenberger, Explicit-solvent molecular dynamics simulations of a reversibly-folding  $\beta$ -heptapeptide in methanol: influence of the treatment of long-range electrostatic interactions, *J. Phys. Chem. B* 113 (2009) 3112.
- [58] A.H. de Vries, I. Chandrasekhar, W.F. van Gunsteren, P.H. Hünenberger, Molecular dynamics simulations of phospholipid bilayers: influence of artificial periodicity, system size, and simulation time, *J. Phys. Chem.* 109 (2005) 11643.
- [59] D.H. Herce, A.E. Garcia, Correction of apparent finite size effects in the area per lipid of lipid membranes simulations, *J. Chem. Phys.* 125 (2006) 224711.
- [60] T. Baştug, S.M. Patra, S. Kuyucak, Finite system and periodicity effects in free energy simulations of membrane proteins, *Chem. Phys. Lett.* 425 (2006) 320.
- [61] D.P. Tielemans, S.J. Marrink, H.J.C. Berendsen, A computer perspective of membranes: molecular dynamics studies of lipid bilayers systems, *Biochim. Biophys. Acta* 1331 (1997) 235.
- [62] J.B. Klauda, B.R. Brooks, R.W. Pastor, Dynamical motions of lipids and a finite size effect in simulations of bilayers, *J. Chem. Phys.* 125 (2006) 144710.
- [63] S. Nagarajan, E.E. Schuler, K. Ma, J.T. Kindt, R.B. Dyer, Dynamics of the gel to fluid phase transformation in unilamellar DPPC vesicles, *J. Phys. Chem. B* 116 (2012) 13749.
- [64] M. Laner, P.H. Hünenberger, Effect of methanol on the phase-transition properties of glycerol-monopalmitate lipid bilayers investigated using molecular dynamics simulations: in quest of the biphasic effect, *J. Mol. Graph. Model.* 55 (2015) 85.
- [65] M. Laner, P.H. Hünenberger, Thermodynamics and kinetics of the gel to liquid-crystal phase transitions in glycerol-monopalmitate lipid bilayers: a Markov model analysis based on atomistic molecular dynamics simulations, *J. Chem. Theory Comput.* (2014), submitted for publication.
- [66] W.R. Hargreaves, S.J. Mulvihill, Deamer, Synthesis of phospholipids and membranes in prebiotic conditions, *Nature* 3 (1976) 78.
- [67] F. Olasagasti, M.-C. Maurel, Deamer, Physico-chemical interactions between compartment forming lipids and other prebiotically relevant biomolecules, *BIO Web of Conferences* 2 (2014) 05001.
- [68] N. Krog, K. Larsson, Phase behaviour and rheological properties of aqueous systems of industrial distilled monoglycerides, *Chem. Phys. Lipids* 2 (1968) 129.
- [69] W.G. Morley, G.J.T. Tiddy, Phase behavior of monoglyceride/water systems, *J. Chem. Soc. Faraday Trans.* 89 (1993) 2823.
- [70] A.H. de Vries, S. Yefimov, A.E. Mark, S.J. Marrink, Molecular structure of the lecithin ripple phase, *Proc. Natl. Acad. Sci. U. S. A.* 102 (2005) 5392.
- [71] N. Krog, A.P. Borup, Swelling behaviour of lamellar phases of saturated monoglycerides in aqueous systems, *J. Sci. Food Agric.* 24 (1973) 691.
- [72] I. Pezon, E. Pezon, B.A. Bergenstahl, P.M. Claesson, Repulsive pressure between monoglyceride bilayers in the lamellar and gel states, *J. Phys. Chem.* 94 (1990) 8255.
- [73] I. Pezon, E. Pezon, P.M. Claesson, B.A. Bergenstahl, Monoglyceride surface films: stability and interlayer interactions, *J. Colloid Interface Sci.* 144 (1991) 449.
- [74] G. Cassin, C. de Costa, J.P.M. van Duynhoven, W.G.M. Agterof, Investigation of the gel to coagel phase transition in monoglyceride–water systems, *Langmuir* 14 (1998) 5757.
- [75] A. Stein, J.A. Verheij, W.G.M. Agterof, Rheological characterization, crystallization, and gelation behavior of monoglyceride gels, *J. Colloid Interface Sci.* 249 (2002) 412.
- [76] J.P.M. van Duynhoven, I. Broekmann, A. Stein, G.M.P. van Kempen, G.-J.W. Goudappel, W.S. Veeman, Microstructural investigation of monoglyceride–water coagel systems by NMR and CryoSEM, *J. Colloid Interface Sci.* 285 (2005) 703.
- [77] A. Alberola, B. Blümich, D. Emeis, K.-P. Wittern, Phase transitions of monoglyceride emulsifier systems and pearlescent effects in cosmetic creams studied by  $^{13}\text{C}$  NMR spectroscopy and DSC, *Colloids Surf. A: Physicochem. Eng. Aspects* 290 (2006) 247.
- [78] N. Schmid, C.D. Christ, M. Christen, A.P. Eichenberger, W.F. van Gunsteren, Architecture, implementation and parallelisation of the GROMOS software for biomolecular simulation, *Comput. Phys. Commun.* 183 (2012) 890.
- [79] A.-P.E. Kunz, J.R. Allison, D.P. Geerke, B.A.C. Horta, P.H. Hünenberger, S. Riniker, N. Schmid, W.F. van Gunsteren, New functionalities in the GROMOS biomolecular simulation software, *J. Comput. Chem.* 33 (2012) 340.
- [80] W.F. van Gunsteren, The GROMOS software for biomolecular simulation. Available from: <http://www.gromos.net> (accessed 05.05.11).
- [81] B.A.C. Horta, P.F.J. Fuchs, W.F. van Gunsteren, P.H. Hünenberger, New interaction parameters for oxygen compounds in the GROMOS force field: improved pure-liquid and solvation properties for alcohols, ethers, aldehydes, ketones, carboxylic acids and esters, *J. Chem. Theor. Comput.* 7 (2011) 1016.
- [82] H.J.C. Berendsen, J.P.M. Postma, W.F. van Gunsteren, J. Hermans, Interaction models for water in relation to protein hydration, in: B. Pullman (Ed.), *Intermolecular Forces*, Reidel, Dordrecht, The Netherlands, 1981, pp. 331–342.
- [83] H.J.C. Berendsen, J.P.M. Postma, W.F. van Gunsteren, A. di Nola, J.R. Haak, Molecular dynamics with coupling to an external bath, *J. Chem. Phys.* 81 (1984) 3684.
- [84] W.F. van Gunsteren, H.J.C. Berendsen, Computer simulation of molecular dynamics: methodology, applications and perspectives in chemistry, *Angew. Chem. Int. Ed.* 29 (1990) 992.
- [85] W.F. van Gunsteren, S.R. Billeter, A.A. Eising, P.H. Hünenberger, P. Krüger, A.E. Mark, W.R.P. Scott, I.G. Tironi, *Biomolecular Simulation: The GROMOS96 Manual and User Guide*, Verlag der Fachvereine, Zürich, Switzerland, 1996.
- [86] J.A. Barker, R.O. Watts, Monte Carlo studies of the dielectric properties of water-like models, *Mol. Phys.* 26 (1973) 789.
- [87] I.G. Tironi, R. Sperb, P.E. Smith, W.F. van Gunsteren, A generalized reaction field method for molecular dynamics simulations, *J. Chem. Phys.* 102 (1995) 5451.
- [88] P.F.H. Franck, E.M. Bevers, B.H. Lubin, P. Comfurius, D.T.-Y. Chiu, J.A.F. Op den Kamp, R.F.A. Zwaal, L.L.M. van Deenen, B. Roelofs, Uncoupling of the membrane skeleton from the lipid bilayer, *J. Clin. Invest.* 75 (1985) 183.
- [89] P.F. Devaux, Lipid transmembrane asymmetry and flip-flop in biological membranes and in lipid bilayers, *Curr. Opin. Struct. Biol.* 3 (1993) 489.
- [90] F. Kamp, D. Zakim, D. Zhand, N. Noy, J.A. Hamilton, Fatty acid flip-flop in phospholipid bilayers is extremely fast, *Biochemistry* 34 (1995) 11928.
- [91] A.M. Kleinfeld, P. Chu, C. Romero, Transport of long-chain native fatty acids across lipid bilayer membranes indicates that transbilayer flip-flop is rate limiting, *Biochemistry* 36 (1997) 14146.
- [92] J.A. Hamilton, S.P. Bhamidipati, D.R. Kodali, D.M. Small, The interfacial conformation and transbilayer movement of diacylglycerols in phospholipid bilayers, *J. Biol. Chem.* 266 (1991) 1177.
- [93] J. Katsaras, D.S.C. Yang, R.M. Epand, Fatty-acid chain tilt angles and directions in dipalmitoyl phosphatidylcholine bilayers, *Biophys. J.* 63 (1992) 1170.
- [94] W.F.D. Bennett, J.L. MacCallum, M.J. Hinner, S.J. Marrink, D.P. Tielemans, Molecular view of cholesterol flip-flop and chemical potential in different membrane environments, *J. Am. Chem. Soc.* 131 (2009) 12714.
- [95] R. Chen, D. Poger, A.E. Mark, Effect of high pressure on fully hydrated DPPC and POPC bilayers, *J. Phys. Chem. B* 115 (2011) 1038.
- [96] F. Yarrow, T.J.H. Vlugt, J.P.J.M. van der Eerden, M.M.E. Snel, Melting of a DPPC lipid bilayer observed with atomic force microscopy and computer simulation, *J. Cryst. Growth* 275 (2005) 1417.
- [97] D.M. Small, Lateral chain packing in lipids and membranes, *J. Lipid Res.* 25 (1984) 1490.
- [98] H. Schindler, J. Seelig, Deuterium order parameters in relation to thermodynamic properties of a phospholipid bilayer. A statistical mechanical interpretation, *Biochemistry* 14 (1975) 2283.
- [99] J.-P. Douliez, A. Léonard, E.J. Dufourc, Restatement of order parameters in biomembranes: calculation of C–C bond order parameters from C–D quadrupolar splittings, *Biophys. J.* 68 (1995) 1727.
- [100] L.S. Vermeer, B.L. de Groot, V. Reat, A. Milon, J. Czaplicki, Acyl chain order parameter profiles in phospholipid bilayers: computation from molecular dynamics simulations and comparison with  $^2\text{H}$  NMR experiments, *Eur. Biophys. J.* 36 (2007) 919.
- [101] T.T. Mills, G.E.S. Toombes, S. Tristram-Nagle, D.-M. Smilgies, G.W. Feigenson, J.F. Nagle, Order parameters and areas in fluid-phase oriented lipid membranes using wide angle X-ray scatterin, *Biophys. J.* 95 (2008) 669.
- [102] J.-P. Douliez, A. Léonard, E.J. Dufourc, Conformational order of DMPC sn-1 versus sn-2 chains and membrane thickness: an approach to molecular protrusion by solid state  $^2\text{H}$ -NMR and neutron diffraction, *J. Phys. Chem.* 100 (1996) 18450.
- [103] F.Y. Jiang, Y. Bouret, J.T. Kindt, Molecular dynamics simulations of the lipid bilayer edge, *Biophys. J.* 87 (2004) 182.

- [104] G.J.T. Tiddy, Surfactant-water liquid crystal phases, *Phys. Rep.* 57 (1980) 1.
- [105] I. Pascher, M. Lundmark, P.-G. Nyholm, S. Sundell, Crystal structure of membrane lipids, *Biochim. Biophys. Acta* 1113 (1992) 339.
- [106] J.F. Nagle, Theory of biomembrane phase transitions, *J. Chem. Phys.* 58 (1973) 252.
- [107] J.F. Nagle, Theory of lipid monolayer and bilayer phase transitions: effect of headgroup interactions, *J. Membr. Biol.* 27 (1976) 233.
- [108] I. Pascher, The different conformations of the glycerol region of crystalline acylglycerol, *Curr. Opin. Struct. Biol.* 6 (1996) 439.
- [109] M. Kranenburg, M. Vlaar, B. Smit, Simulating induced interdigitation in membranes, *Biophys. J.* 87 (2004) 1596.
- [110] S.-S. Qin, Z.-W. Yu, Y.-X. Yu, Structural characterization on the gel to liquid-crystal phase transition of fully hydrated DSPC and DSPE bilayers, *J. Phys. Chem. B* 113 (2009) 8114.
- [111] N. Nandi, D. Vollhardt, Effect of molecular chirality on the morphology of biomimetic Langmuir monolayers, *Chem. Rev.* 103 (2003) 4033.
- [112] Y.G. Smirnova, S.-J. Marrink, R. Lipowski, V. Knecht, Solvent-exposed tails as prestalk transition states for membrane fusion at low hydration, *J. Am. Chem. Soc.* 132 (2010) 6710.
- [113] T.J. Piggot, D.A. Holdbrook, S. Khalid, Electroporation of the *E. coli* and *S. aureus* membranes: molecular dynamics simulations of complex bacterial membranes, *J. Phys. Chem. B* (2011) 115.